U.S. DEPARTMENT OF ENERGY

PNNL-17878

Prepared for the U.S. Department of Energy
under Contract DE-AC05-76RL01830

Improved Predictions of Carbon Tetrachloride Contaminant Flow and Transport: Implementation of Kinetic Volatilization and Multicomponent NAPL Behavior

M Oostrom
VL Freedman
F Zhang
GD Tartakovsky

September 2008

Pacific Northwest
NATIONAL LABORATORY

DISCLAIMER

PACIFIC NORTHWEST NATIONAL LABORATORY
operated by
BATTELLE
for the
UNITED STATES DEPARTMENT OF ENERGY
under Contract DE-AC05-76RL01830

Printed in the United States of America

Available to DOE and DOE contractors from the
Office of Scientific and Technical Information,
P.O. Box 62, Oak Ridge, TN 37831-0062;
ph: (865) 576-8401
fax: (865) 576-5728
email: reports@adonis.osti.gov

Available to the public from the National Technical Information Service,
U.S. Department of Commerce, 5285 Port Royal Rd., Springfield, VA 22161
ph: (800) 553-6847
fax: (703) 605-6900
email: orders@ntis.fedworld.gov
online ordering: http://www.ntis.gov/ordering.htm


This document was printed on recycled paper.
(9/2003)

PNNL-17878

Improved Predictions of Carbon Tetrachloride Contaminant Flow and Transport: Implementation of Kinetic Volatilization and Multicomponent NAPL Behavior

M Oostrom
VL Freedman
F Zhang
GD Tartakovsky

September 2008

Prepared for
the U.S. Department of Energy
under Contract DE-AC05-76RL01830

Pacific Northwest National Laboratory
Richland, Washington 99352

Abstract

Carbon tetrachloride (CT) was discharged to waste sites that are included in the 200-PW-1 Operable Unit in Hanford 200 West Area. Fluor Hanford, Inc. is conducting a Comprehensive Environmental Response, Compensation, and Liability Act (CERCLA) remedial investigation/feasibility study (RI/FS) for the 200-PW-1 Operable Unit. The RI/FS process and remedial investigations for the 200-PW-1, 200-PW-3, and 200-PW-6 Operable Units are described in the Plutonium/Organic-Rich Process Condensate/Process Waste Groups Operable Unit RI/FS Work Plan. As part of this overall effort, Pacific Northwest National Laboratory (PNNL) was contracted to improve the STOMP simulator (White and Oostrom, 2006) by incorporating kinetic volatilization of nonaqueous phase liquids (NAPL) and multicomponent flow and transport. This work supports the U.S. Department of Energy's (DOE's) efforts to characterize the nature and distribution of CT in the 200 West Area and subsequently select an appropriate final remedy.

Previous numerical simulation results with the STOMP simulator have overestimated the effect of soil vapor extraction (SVE) on subsurface CT, showing rapid removal of considerably more CT than has actually been recovered so far. These previous multiphase simulations modeled CT mass transfer between phases based on equilibrium partitioning. Equilibrium volatilization can overestimate volatilization because mass transfer limitations present in the field are not considered. Previous simulations were also conducted by modeling the NAPL as a single component, CT. In reality, however, the NAPL mixture disposed of at the Hanford site contained several non-volatile and nearly insoluble organic components, resulting in time-variant fluid properties as the CT component volatilized or dissolved over time. Simulation of CT removal from a DNAPL mixture using single-component DNAPL properties typically leads to an overestimation of CT removal. Other possible reasons for the discrepancy between observed and simulated CT mass removal during SVE are differences between the actual and simulated 1) SVE flow rates, 2) fluid-media properties, and 3) disposal history (volumes, rates, and timing).

In this report, numerical implementation of kinetic volatilization and multicomponent DNAPL flow and transport into the STOMP simulator (White and Oostrom, 2006) is described. The results of several test cases are presented and explained. The addition of these two major code enhancements increases the ability of the STOMP simulator to model complex subsurface flow and transport processes involving CT at the Hanford site.

Acknowledgments

This work was completed for the project “PNNL Support to Technical Integration & Assessment for FY08” under Fluor Hanford Inc. (FHI) Contract No. 27647, Release No. 306, Amendment No. 7. The support of Chris Sutton, FHI, to enhance the STOMP simulator with the capabilities described in this report is appreciated. The authors acknowledge the constructive comments by reviewer Mike Truex. This report has not been reviewed by FHI before publication.

Contents

Abstract iii
Acknowledgments v
1.0 Introduction 1.1
2.0 Numerical Model Description 2.1
2.1 Numerical Model 2.1
3.0 NAPL Kinetic Volatilization and Dissolution 3.1
3.1 Background 3.1
3.1.1 NAPL Volatilization 3.1
3.1.2 NAPL Dissolution 3.2
3.1.3 Objectives 3.2
3.2 Mathematical Relations 3.2
3.2.1 Continuity Equations 3.2
3.2.2 Kinetic Volatilization Models 3.4
3.2.3 Kinetic Dissolution Models 3.8
3.3 STOMP Modifications 3.10
3.3.1 Summary of Modification 3.10
3.3.2 Assumptions 3.10
3.3.3 Summary of Subroutine Modification 3.10
3.3.4 Input Modification 3.11
3.4 Code Evaluation 3.11
3.5 Test Results 3.12
3.5.1 Quantitative Evaluation 3.12
3.5.2 Qualitative Evaluation 3.15
3.5.3 Test Summary 3.24
4.0 Multicomponent NAPL Formulation 4.1
4.1 Computation of Multicomponent Parameter Values 4.1
4.1.1 Aqueous-Phase Density 4.2
4.1.2 NAPL-Phase Density 4.2
4.1.3 Gas-Phase Density 4.3
4.1.4 Gas-Phase Viscosity 4.4
4.1.5 Aqueous-Phase Viscosity 4.5
4.1.6 NAPL-Phase Viscosity 4.5
4.1.7 NAPL-Phase Component Fractions 4.5
4.2 Test Cases 4.6
4.2.1 Cases 1 and 2 4.8
4.2.2 Case 3 4.11

4.2.3 Case 4 ..... 4.14
4.2.4 Case 5 ..... 4.18
4.2.5 Case 6 ..... 4.22
4.2.6 Test Summary 4.25
5.0 Summary and Conclusions 5.1
6.0 References 6.1
Appendix A – STOMP Input File for the Base Case Kinetic Volatilization Simulation Scenario Using the Wilkins Model A.1
Appendix B – STOMP Input File for Case 1a Multicomponent Simulation B.1

Figures

1.1 Carbon Tetrachloride Mass (kg) Distribution in the DNAPL, Aqueous and Gaseous Phases, and Sorbed to the Solid phase for the Base Case Simulation.. ..... 1.2

3.1 Comparison of the Wilkins et al. (1995), the van der Ham and Brouwers (1998), and the Yoon et al. (2002) Models for $0.01 \leq P_e^g \leq 100$ for Three Soils of Different Mean Particle Size. 3.7

3.2 (a) and (b) Comparison of the Equilibrium, Wilkins (1995), Yoon et al. (2002), the van der Ham and Brouwers (1998) Models (Case 1); (c) and (d) Comparison of the Equilibrium Model and Those with Constant k_v values, $k_v\_1 = 0.0001\ s^{-1}$, $k_v\_2 = 0.001\ s^{-1}$, and $k_v\_3 = 0.01\ s^{-1}$ (Case 2) 3.16

3.3 Effects of mean particle diameter (d_{50}) on NAPL volatilization. (a) and (b) $d_{50} = 0.002$ cm (Case 3), (c) and (d) $d_{50} = 0.02$ cm (Case 1), and (e) and (f) $d_{50} = 0.2$ cm (Case 4) 3.17

3.4 Effects of Gas Velocity on the Cumulated Gas Oil Migrated out of the Domain. (a) Gas Pressure Gradient = 20 Pa/m (Case 5); (b) Gas Pressure Gradient = 100 Pa/m (Case 1), (c) Gas Pressure Gradient = 500 Pa/m (Case 6), (d) Gas Pressure Gradient = 20, 100 and 500 Pa/m for $t < 0.1$ d, $0.1 \leq t \leq 0.2$, and $t > 0.2$ day, Respectively (Case 7), and (e) Gas Pressure Gradient = 500, 100 and 20 Pa/m for $t < 0.03$ d, $0.03 \leq t \leq 0.1$, and $t > 0.1$ day, Respectively (Case 8) 3.18

3.5 Effects of Gas Velocity on the Gas Oil Concentration. (a) Gas Pressure Gradient = 20 Pa/m (Case 5); (b) Gas Pressure Gradient = 100 Pa/m (Case 1), (c) Gas Pressure Gradient = 500 Pa/m (Case 6), (d) Gas Pressure Gradient = 20, 100 and 500 Pa/m for $t < 0.1$ d, $0.1 \leq t \leq 0.2$, and $t > 0.2$ day, Respectively (Case 7), and (e) Gas Pressure Gradient = 500, 100 and 20 Pa/m for $t < 0.03$ d, $0.03 \leq t \leq 0.1$, and $t > 0.1$ day, Respectively (Case 8) 3.19

3.6 Effects of Aqueous Velocity on the Aqueous Oil Concentration. Aqueous Hydraulic Gradients Were (a) and (b) 500 Pa/m (Case 9), (c) and (d) 1000 Pa/m (Case 10), and (e) and (f) 2000 Pa/m (Case 11) 3.21

3.7 Effects of a Gas Source on NAPL Volatilization. Gas Source Release Rate: (a) and (b) 100 L/d (Case 12); and (c) and (d) 1000 L/d (Case 13) 3.22

3.8 Effects of an Aqueous Source on NAPL Dissolution. Aqueous Source Release Rates: (a) and (b) 100 L/d (Case 14) and (c) and (d) 1000 L/d (Case 15) 3.23

3.9 Volatilization and Dissolution of a NAPL Source. NAPL Source Strength and Duration: (a) and (c) 0.2 L/d for 0.25 d (Case 16), and (b) and (d) 0.2 L/d for 0.5 d (Case 17) 3.24

4.1 Comparison of NAPL Saturations Computed with the Single Component and Multicomponent versions of STOMP for Case 1a 4.10

4.2 NAPL Saturations at t = 30 days for Cases 1a, 1e, 1f, and 1g 4.11

4.3 NAPL Saturations at Various Times for Multicomponent and Single Component Simulations (Case 3a) 4.12

4.4 NAPL Saturations at Various Times for Multicomponent and Single Component Simulations (Case 3b) 4.13

4.5 NAPL Saturations at Various Times for Multicomponent and Single Component Simulations (Case 3c) 4.14

4.6 NAPL Saturations at Various Times for Multicomponent and Single Component Simulations (Case 4a) 4.15

4.7 NAPL Saturations at Various Times for Multicomponent and Single Component Simulations (Case 4b) 4.15
4.8 NAPL Saturations at Various Times for Multicomponent and Single Component Simulations (Case 4c) 4.16
4.9 Comparison of Cases 4a and 4d at 30 Days 4.16
4.10 Comparison of Cases 4a, 4e, and 4f at 30 Days 4.17
4.11 Comparison of Cases 4a, 4g, and 4h at 7 Days 4.17
4.12 Comparison of Cases 4a, 4i, and 4j at 30 Days 4.18
4.14 NAPL Saturations at Various Times for Case 5a Multicomponent Simulation 4.19
4.15 NAPL Saturations at Various Times for Case 5b Multicomponent Simulation 4.20
4.16 Mass and Mole Fractions for Case 5b at 4 Weeks 4.20
4.17 NAPL Saturations at Various Times for Case 5c Multicomponent Simulation 4.21
4.18 Mass and Mole Fractions for Case 5c at 4 Weeks 4.21
4.19 NAPL Saturations at 24 Hours for Case 6a Single Component Simulation 4.22
4.20 NAPL Saturations at 24 Hours for Case 6a Multicomponent Simulation 4.23
4.21 NAPL Saturations at 10 Years for Case 6b Single Component Simulation 4.23
4.22 NAPL Saturations at 10 Years for Case 6b Multicomponent Simulation 4.24
4.23 NAPL Saturations at 24 Hours for Case 6c Single Component Simulation 4.24
4.24 NAPL Saturations at 24 Hours for Case 6c Multicomponent Simulation 4.25

Tables

3.1 NAPL-Aqueous Phase Mass Transfer Correlations Developed after 1990 ..... 3.9
3.2 Description of Test Cases for Kinetic Volatilization Model..... 3.13
3.3 Description of Simulation Scenarios 3.14
3.4 Kinetic Volatilization and Dissolution Coefficients 3.14
3.5 Oil Mass Balance at the End of Simulation 3.14
4.1. Description of Test Cases for Multicomponent NAPL Formulation 4.6

1.0 Introduction

Plutonium recovery operations within the Z-Plant aggregate area (Plutonium Finishing Plant [PFP]) of the Hanford Site resulted in organic and aqueous wastes that were disposed of at several cribs, tile fields, and French drains. The organic wastes consisted of carbon tetrachloride (CT) mixed with lard oil, tributyl phosphate (TBP), and dibutyl butyl phosphonate (DBBP). The main disposal areas were the 216-Z-9 trench, the 216-Z-1A tile field, and the 216-Z-18 crib. The three major disposal facilities received a total of about 13,400,000 L of liquid waste containing 363,000 to 580,000 L of CT.

In recent years, two major remediation technologies have been applied to remove CT from the vadose zone and groundwater at Hanford. Since 1991, about 78,000 kg of CT was removed using a soil vapor extraction (SVE) system in the vadose zone (Fluor Hanford, 2005). In addition, a pump-and-treat system for the unconfined aquifer removed 9,700 kg of CT from groundwater since 1994 (DOE, 2005).

Numerical simulations were conducted to investigate the effect of the SVE on the CT mixture in the subsurface of the disposal sites by Oostrom et al., 2004, 2006a, 2006b, 2007a, 2007b and by White et al., (2008). The detailed multiphase simulations show that the SVE, based on CT equilibrium partitioning between the various phases, should have been quite effective. Applying the averaged extraction rates over the periods when the extraction system was active, yield an almost complete removal of the CT in the dense nonaqueous phase liquid (DNAPL), sorbed to the solid phase, and dissolved in the aqueous and gas phases. The simulated SVE was also sufficient to remove CT from the Cold Creek unit. These results are in contrast to field observations and significantly overestimated the amount of CT mass extracted from the vadose zone. An example of the rapid simulated removal of CT after activation in 1993 is shown in Figure 1.1 (from Oostrom et al., 2007b).

There are several possible reasons for this discrepancy, including differences between the actual and simulated 1) SVE flow rates, 2) fluid-media properties, and 3) disposal history (volumes, rates, and timing). Differences may also be due, in part, because these previous multiphase simulations modeled CT mass transfer between phases based on equilibrium partitioning. Equilibrium volatilization can overestimate volatilization because mass transfer limitations present in the field are not considered. Furthermore, the previous simulations assume that the DNAPL had constant properties. In reality, however, the DNAPL contains a mixture of several non-volatile and nearly insoluble organic components along with CT, resulting in time-variant fluid properties as the CT component volatilized or dissolved over time. Simulation of CT removal from a DNAPL mixture using single-component DNAPL properties typically leads to an overestimation of CT removal (Oostrom et al., 2007a).

In this report, numerical implementation of kinetic volatilization and multicomponent DNAPL flow and transport into the STOMP simulator (White and Oostrom, 2006) is described. The results of several test cases are presented and explained.

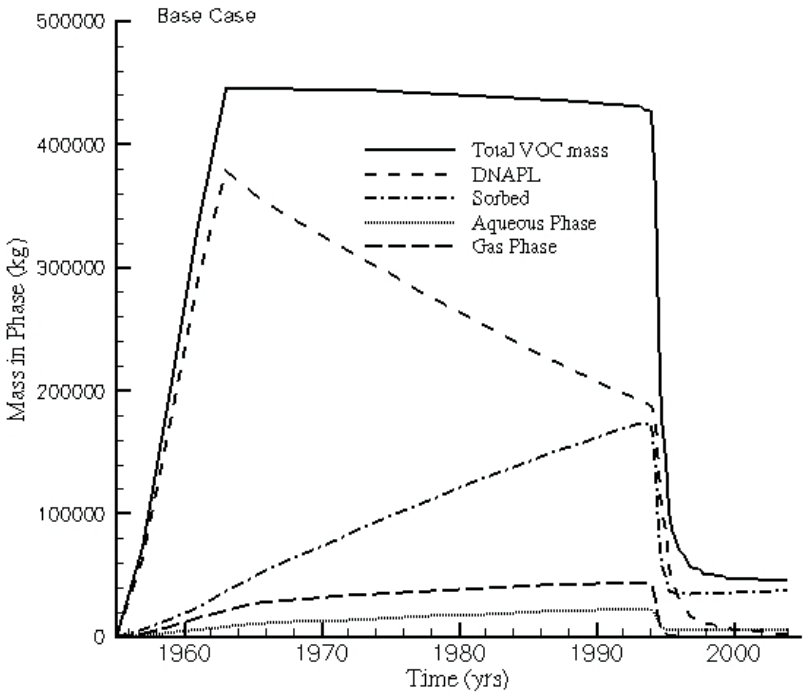

Figure 1.1. Carbon Tetrachloride Mass (kg) Distribution in the DNAPL, Aqueous and Gaseous Phases, and Sorbed to the Solid phase for the Base Case Simulation. VOC = Volatile Organic Carbon (from Oostrom et al., 2007b).

2.0 Numerical Model Description

2.1 Numerical Model

The modifications for the kinetic volatilization enhancement were made in the water-oil-air operational mode (STOMP-WOA) of the STOMP simulator (White and Oostrom 2006). The fully implicit integrated finite difference code has been used to simulate a variety of multifluid systems (e.g., Oostrom et al. 1997, 1999; Oostrom and Lenhard 1998; Schroth et al. 1998; Oostrom et al., 2007; White et al., 2008). The applicable governing equations are the component mass-conservation equations for water, organic compounds, and air, expressed as:

$$\frac{\partial}{\partial t}\left[n_D \omega_l^w \rho_l s_l\right] = -\nabla F_l^w + \dot{m}^w \tag{2.1a}$$

$$\frac{\partial}{\partial t}\left[\sum_{\gamma=l,n,g}\left(n_D \omega_\gamma^o \rho_\gamma s_\gamma\right) + \left((1-n_T)\omega_s^o \rho_s\right)\right] = -\sum_{\gamma=l,n,g}\left\{\nabla F_\gamma^o + \nabla J_\gamma^o\right\} + \dot{m}^o \tag{2.1b}$$

$$\frac{\partial}{\partial t}\left[\sum_{\gamma=l,g}\left(n_D \omega_\gamma^a \rho_\gamma s_\gamma\right)\right] = -\sum_{\gamma=l,g}\left\{\nabla F_\gamma^a + \nabla J_\gamma^a\right\} + \dot{m}^a \tag{2.1c}$$

where

$$F_\gamma^w = -\frac{\omega_\gamma^w \rho_\gamma k_{rl} k}{\mu_\gamma}\left(\nabla P_\gamma + \rho_\gamma g z\right) \text{ for } \gamma = \text{l,g,} \tag{2-1d}$$

$$F_\gamma^o = -\frac{\omega_\gamma^o \rho_l k_{r\gamma} k}{\mu_\gamma}\left(\nabla P_\gamma + \rho_\gamma g z\right) \text{ for } \gamma = \text{l,n,g} \tag{2.1e}$$

$$F_\gamma^a = -\frac{\omega_\gamma^a \rho_\gamma k_{r\gamma} k}{\mu_\gamma}\left(\nabla P_\gamma + \rho_\gamma g z\right) \text{ for } \gamma = \text{l,g} \tag{2.1f}$$

$$J_\gamma^w = -\tau_\gamma n_D \rho_\gamma s_\gamma \frac{M^w}{M_\gamma} D_\gamma^w \nabla \chi_\gamma^w \text{ for } \gamma = \text{l,g} \tag{2.1g}$$

$$J_\gamma^o = -\tau_\gamma n_D \rho_\gamma s_\gamma \frac{M^o}{M_\gamma} D_\gamma^o \nabla \chi_\gamma^o \text{ for } \gamma = \text{l,n,g} \tag{2.1h}$$

$$J_\gamma^a = -\tau_\gamma n_D \rho_\gamma s_\gamma \frac{M^a}{M_\gamma} D_\gamma^a \nabla \chi_\gamma^a \text{ for } \gamma = \text{l,g} \tag{2.1i}$$

The subscripts l, n, g, and s denote aqueous, NAPL, gas and solid phases, respectively; the superscripts w, o, and a denote water, organic compound, and air components, respectively; t is time (s), n_D is the diffusive porosity, n_T is the total porosity, ω is the component mass fraction, ρ is the density (kg/m^3), s is the actual liquid saturation, V is the volumetric flux (m/s), J is the diffusive-dispersive mass flux vector (kg/m^{2}s), m is the component mass source rate (kg/m^{3}s), k is the intrinsic permeability (m^2), $k_{r\gamma}$ is the relative permeability of phase γ, μ is the viscosity (Pa s), P is the pressure (Pa), g_z is the gravitational vector (m/s^2), τ is the tortuosity, M is the molecular weight (kg/mole), D is the diffusive-dispersive tensor (m^2/s), and χ is the component mole fraction. The partitioning between the aqueous and solid phases is described by a linear exchange isotherm through a constant distribution coefficient.

The governing partial differential equations (Equations 2.1a, 2.1b, and 2.1c) are discretized following the integrated-volume finite difference method by integrating over a control volume. Using Euler backward time differencing, yielding a fully implicit scheme, a series of nonlinear algebraic expressions is derived. The algebraic forms of the nonlinear governing equations are solved with a multi-variable, residual-based Newton-Raphson iterative technique, where the Jacobian coefficient matrix is composed of the partial derivatives of the governing equations with respect to the primary variables.

Assuming the aqueous phase never disappears, the primary variable for the water equation is always the aqueous pressure. For the oil equation, the primary variable is P_n when free NAPL is present, s_n when only entrapped NAPL is present, and the component mole fraction when no NAPL is present. For the air equation, the primary variable is P_a. The algebraic expressions are evaluated using upwind interfacial averaging to fluid density, mass fractions, and relative permeability. Specified weights (i.e., arithmetic, harmonic, geometric, upwind) are applied to the remaining terms of the flux equations. For the simulations described in this report, harmonic averages were used and the maximum number of Newton-Raphson iterations was 16, with a convergence factor of 10^{-6}.

Secondary variables, those parameters not directly computed from the solution of the governing equations, are computed from the primary variable set through the constitutive relations. In this section, only the relations between relative permeability, fluid saturation, and capillary pressure (*k-S-P*) pertinent to the conducted simulations are described. The *k-S-P* relations consist of the Brooks and Corey (1964) S-P relations in combination with the k-S relations derived from the Burdine (1953) or Mualem (1976) model. In these relations, the effects of fluid entrapment and residual saturation formation have been included.

The *k-S-P* relations distinguish between actual, effective, and apparent saturations. Actual saturations are defined as the ratio of fluid volume to diffusive pore volume. Effective saturations represent normalized actual saturations based on the pore volumes above the irreducible or minimum saturation of the wetting fluid (i.e., aqueous phase liquid). Effective saturations for the aqueous phase, NAPL, and gas phases and the total liquid are defined according to Equation (2.2):

$$\bar{s}_l = \frac{s_l - s_{rl}}{1 - s_{rl}} \tag{2.2a}$$

$$\bar{s}_n = \frac{s_n}{1 - s_{rl}} \tag{2.2b}$$

$$\bar{s}_g = \frac{s_g}{1 - s_{rl}} \tag{2.2c}$$

$$\bar{s}_t = \frac{s_l + s_n - s_{rl}}{1 - s_{rl}} \tag{2.2d}$$

where s_{rl} is the irreducible aqueous phase saturation. Apparent saturations are defined in terms of effective saturations. Apparent saturations represent the effective saturation of the fluid plus the effective saturations of fluids of lesser wettability entrapped within the wetting fluid. In the simulator, it is assumed that fluid wettability follows the sequence: water > NAPL > air (Leverett 1941). Fluids of lesser wettability can potentially be trapped by NAPL or aqueous phase, and NAPL can be entrapped by the aqueous phase.

In a three-phase system, the apparent total-liquid saturation is considered to be a function of the air-NAPL capillary pressure, and the apparent aqueous phase saturation a function of the NAPL-water capillary pressure, as follows:

$$\bar{\bar{s}}_t = \left[\frac{P_d}{\beta_{gn} P_{gn}}\right]^{\lambda} \quad \text{for} \quad \beta_{gn} P_{gn} > P_d \tag{2-3a}$$

$$\bar{\bar{s}}_t = 1 \quad \text{for} \quad \beta_{gn} P_{gn} \le P_d \tag{2-3b}$$

$$\bar{\bar{s}}_l = \left[\frac{P_d}{\beta_{nl} P_{nl}}\right]^{\lambda} \quad \text{for} \quad \beta_{nl} P_{nl} > P_d \tag{2-3c}$$

$$\bar{\bar{s}}_l = 1 \quad \text{for} \quad \beta_{nl} P_{nl} \le P_d \tag{2-3d}$$

where P_d is the air-entry pressure, P_{gn} the gas phase – NAPL capillary pressure, P_{nl} the NAPL – aqueous phase capillary pressure, γ is a pore-size distribution factor, and β_{gn} and β_{nl} are interfacial tension dependent scaling factors, defined as $\beta_{gn} = (\sigma_{gn} - \sigma_{nl}) / \sigma_{gn}$ and $\beta_{nl} = (\sigma_{gn} - \sigma_{nl}) / \sigma_{nl}$, respectively. The nature of these relations is discussed by Lenhard (1994). For aqueous-gas phase systems, Equation (2.3) is replaced by

$$\bar{\bar{s}}_l = \left[\frac{P_d}{P_{gl}}\right]^{\lambda} \quad \text{for} \quad P_{gl} > P_d \tag{2.4a}$$

$$\bar{\bar{s}}_l = 1 \quad \text{for} \quad P_{gl} \le P_d \tag{2.4b}$$

Modeling the subsurface behavior of contaminants can be a cost-effective tool to aid in cleaning up and managing contaminated sites. Before models can be the tools of choice, they must be able to accurately predict contaminant behavior and assess the level of uncertainty associated with the predictions.

The multicomponent enhancements have been implemented in the both water-air-oil and the water-oil operational mode of the STOMP simulator. The water-oil mode requires the assumptions that advective and diffusive-dispersive transport through the gas phase is negligible, isothermal conditions exist, and the NAPL consists of one component. With these assumptions, the applicable governing equations are the component mass-conservation equations for water and organic compounds, expressed as, respectively.

$$\frac{\partial}{\partial t}\left[n_D \omega_l^w \rho_l s_l\right] = -\nabla \mathrm{F}_l^w + \dot{m}^w \tag{2.5a}$$

$$\frac{\partial}{\partial t}\left[\sum_{\gamma=l,n}\left(n_D \omega_\gamma^o \rho_\gamma s_\gamma\right) + \left(1-n_T\right)\omega_s^o \rho_s\right] = -\sum_{\gamma=l,n}\left\{\nabla \mathrm{F}_\gamma^o + \nabla \mathrm{J}_\gamma^o\right\} + \dot{m}^o \tag{2.5b}$$

where

$$\mathrm{F}_l^w = -\frac{\omega_l^w \rho_l k_{rl} \mathrm{k}}{\mu_l}\left(\nabla P_l + \rho_l g \mathrm{z}\right) \tag{2.6a}$$

$$\mathrm{F}_\gamma^o = -\frac{\omega_\gamma^o \rho_\gamma k_{r\gamma} \mathrm{k}}{\mu_\gamma}\left(\nabla P_\gamma + \rho_\gamma g \mathrm{z}\right) \text{ for } \gamma = l, n \tag{2.6b}$$

$$\mathbf{J}_\gamma^o = -\tau_\gamma n_D \rho_\gamma s_\gamma \frac{M^o}{M_\gamma} D_\gamma^o \nabla \chi_\gamma^o \text{ for } \gamma = l, n \tag{2.6c}$$

3.0 NAPL Kinetic Volatilization and Dissolution

3.1 Background

3.1.1 NAPL Volatilization

The SVE technique applies a vacuum to extract contaminated air in connected soil pores. When soil gas concentration decreases, the local chemical equilibrium is perturbed, causing the transfer of volatile oil from the NAPL phase into the soil gas, where it can be removed. Traditionally, an equilibrium mass transfer approach is used to describe NAPL volatilization where the time needed for oil to transfer from the NAPL to the gas phase at local scale is assumed to be very short compared to bulk gas movement (e.g., Corapcioglu and Baehr 1987; Baehr 1987; Wilson et al. 1987; Wilson et al. 1988; Baehr et al. 1989; Johnson et al. 1990). However, an equilibrium mass transfer approach is a maximum rate and can overestimate NAPL volatilization.

Mass transfer limitations typically cause volatilization of NAPL in the subsurface to be a non-equilibrium process. Experimental results using natural geological materials often show effluent concentrations below the theoretical maximum based on contaminant partial pressures (Baehr et al. 1989; Mackay et al. 1990; Rainwater et al., 1989). Gierke et al. (1992) used a mathematical model and laboratory column experiments to examine the impacts of mass partitioning and other factors on subsurface movement of organic vapors. Their results implied that vapor extraction performance will be affected by nonequilibrium transport and prediction of organic contaminant removal by vapor extraction must account for non-equilibrium processes.

Based on the theory in Welty et al. (1984), Rathfelder (1991) described the interphase mass transfer with a kinetic model, which assumes 1) mass transfer is controlled by the rate of diffusion on each side of the interface, and 2) no resistance to transfer is encountered at the interface. Often, the diffusional resistance on one side of the interface is considered dominant so that mass transfer rates can be described with a single overall mass transfer coefficient. Mathematically, the interphase mass transfer can then be described with a first-order rate expression rather than explicitly modeling all the elements of the mass transfer process (e.g., Lingineni and Khir, 1992; Armstrong et al. 1994; Lee et al. 2000; Falta 2000; Anwar et al. 2003; Harper et al. 2003; Abriola et al. 2004; Wilkins et al. 1995; van der Ham and Brouwers 1998; Yoon et al. 2002; Bohy et al. 2006; Rahbeh and Mohtar 2006, 2007).

A first-order rate expression for NAPL volatilization has been used in the SVE simulator MISER to simulate one component (Abriola et al. 1999; Rathfelder et al. 2000) and multi-component (Abriola et al. 2004) NAPL volatilization. These simulators describe the movement of the gas and aqueous phases by standard macroscopically averaged flow equations. The NAPL phase is considered immobile but there is interface mass transfer between the NAPL and the water and gas phases. Coupled nonlinear flow and transport equations are solved where the solution of the organic liquid saturation equation follows after the solution of the transport equations.

Determining the volatilization coefficient for a first-order rate expression in the subsurface is challenging because the coefficient, k_v, is a function of the mean particle diameter, gas velocity, gas diffusivity, NAPL content, and other factors. Hence, researchers empirical models are typically used to estimate k_v. These models generally can be categorized into two types: NAPL-saturation-independent

(NSI) models (e.g., Wilkins et al. 1995; van der Ham and Brouwers 1998; Yoon et al. 2002) and NAPL-saturation-dependent (NSD) models (e.g., Anwar et al. 2003; Harper et al. 2003; van der Ham and Brouwers 1998). Intuitively, the NSD models should behave better than the NSI models. However, due to the complex impact of NAPL saturation on k_v, contradictory results have been found among the NSD models. For example, van der Ham and Brouwers (1998) and Harper et al. (2003) found that k_v increases with increasing NAPL saturation while Anwar et al. (2003) observed the opposite, k_v decreases with increasing NAPL saturation. Because of these inconsistencies, the NSD models of k_v are not considered in this work. Details of the NSI models are presented in the next section.

3.1.2 NAPL Dissolution

Similar to the NAPL volatilization process, both equilibrium and kinetic approaches have been used to describe the NAPL dissolution process. Miller et al. (1990) summarized the NAPL-aqueous phase mass transfer expressions that had been developed up through 1990. More recent expressions, developed after 1990, are summarized in the next section.

3.1.3 Objectives

The primary purpose of this work is to incorporate the capability to simulate kinetic volatilization and dissolution of NAPL into the water-oil-air (WOA) mode of the Subsurface Transport Over Multiple Phases (STOMP) numerical simulator. The revised code enables the user to select either equilibrium or the kinetic models for volatilization and dissolution. Code modifications implemented to meet this objective are evaluated with quantitative and qualitative tests to verify proper operation of the code.

3.2 Mathematical Relations

This section describes the mathematical equations and models for incorporating the kinetic NAPL volatilization and dissolution processes into the WOA mode of the STOMP simulator.

3.2.1 Continuity Equations

To consider NAPL kinetic volatilization and dissolution processes, three coupled continuity equations must be considered, one for the oil component in the NAPL phase, one for the oil vapor in the gas phase, and the other for the dissolved oil in the aqueous phase. For consistency, the equations are written in the format used in the STOMP theory guide (White and Oostrom, 2000, Eqs. 3.4.2 and 3.4.3). The continuity equations for the oil component in the NAPL phase, the volatilized oil in the gas phase, and the dissolved oil in the aqueous phase are written as

$$\frac{\partial}{\partial t}\left(\rho_n s_n n_D\right) = -\nabla \mathbf{F}_n + I^o_{n,g} + I^o_{n,l} + \dot{m}^o \tag{3.1}$$

with

$$\mathbf{F}_n = -\frac{\rho_n k_{rn} \mathbf{k}}{\mu_n}\left(\nabla P_n + \rho_n g \mathbf{z}_g\right)$$

$$I_{n,g}^{o} = -n_D s_g k_{n,g}^{vo}\left(\overline{C}_g^{vo} - C_g^{vo}\right)$$
$$I_{n,l}^{o} = -n_D s_l k_{n,l}^{do}\left(\overline{C}_l^{do} - C_l^{do}\right)$$

$$\frac{\partial}{\partial t}\left(n_D \omega_g^{vo} \rho_g s_g\right) = -\left(\nabla \mathbf{F}_g^{vo} + \nabla \mathbf{J}_g^{vo}\right) + I_{n,g}^{vo} + \dot{m}^{vo}$$

with

$$\mathbf{F}_g^{vo} = -\frac{\omega_g^{vo} \rho_g k_{rg} \mathbf{k}}{\mu_g}\left(\nabla P_g + \rho_g g \mathbf{z}_g\right) \tag{3.2}$$
$$\mathbf{J}_g^{vo} = -\tau_g n_D \rho_g s_g \frac{M^o}{M_g} D_g^{vo} \nabla \chi_g^{vo}$$
$$I_{n,g}^{vo} = -I_{n,g}^{o} = n_D s_g k_{n,g}^{vo}\left(\overline{C}_g^{vo} - C_g^{vo}\right)$$

$$\frac{\partial}{\partial t}\left[n_D \omega_l^{do} \rho_l s_l + (1 - n_T)\omega_s^o \rho_s\right] = -\left(\nabla \mathbf{F}_l^{do} + \nabla \mathbf{J}_l^{do}\right) + I_{n,l}^{do} + \dot{m}^{do}$$

with

$$\mathbf{F}_l^{do} = -\frac{\omega_l^{do} \rho_l k_{rl} \mathbf{k}}{\mu_l}\left(\nabla P_l + \rho_l g \mathbf{z}_l\right) \tag{3.3}$$
$$\mathbf{J}_l^{do} = -\tau_l n_D \rho_l s_l \frac{M^o}{M_l} D_l^{do} \nabla \chi_l^{do}$$
$$I_{n,l}^{do} = -I_{n,l}^{o} = n_D s_l k_{n,l}^{do}\left(\overline{C}_l^{do} - C_l^{do}\right)$$

where the subscript "*l*" denotes for the aqueous phase, "n" for the NAPL phase, and "g" for the gas phase; the superscript "o" denotes for oil, "vo" for volatilized oil, and "do" for dissolved oil; the variables are defined below:

ρ_s, ρ_l, ρ_n, ρ_g	solid, aqueous, NAPL and gas phase densities (M L^{-3})
μ_l, μ_n, μ_g	aqueous, NAPL, and gas phase viscosity (M T^{-1} L^{-1})
s_l, s_n, s_g	aqueous, NAPL, and gas phase saturation (-)
$\mathbf{F}_l^{do}$, $\mathbf{F}_n$, $\mathbf{F}_g^{vo}$	dissolved oil, NAPL, and volatilized oil advection flux vectors (M L^{-3} T^{-1})
$\mathbf{J}_l^{do}$, $\mathbf{J}_g^{vo}$	dissolved and volatilized oil diffusive flux vectors (M L^{-3} T^{-1})
n_T, n_D	total and diffusive porosities (-)
$I_{n,l}^{o}$, $I_{n,g}^{o}$	NAPL-aqueous interphase and NAPL-gas interphase mass transfer rates (M L^{-3} T^{-1})
$\dot{m}^{o}$, $\dot{m}^{vo}$	oil, volatilized oil, and dissolved soil source/sinks (M L^{-3} T^{-1})

$\dot{m}^{do}$,	
k	permeability (L^2)
k_{rl}, k_{rn}, k_{rg}	aqueous, NAPL, and gas phase relative permeability (-)
P_l, P_n, P_g	aqueous, NAPL, and gas phase pressures ($M\ T^{-2}\ L^{-1}$)
g	gravitational acceleration ($L\ T^{-2}$)
$\mathbf{z}_g$	unit gravitational direction vector (-)
$k_{n,l}^{do}, k_{n,g}^{vo}$	NAPL-aqueous and NAPL-gas interphase mass transfer coefficients (T^{-1})
$\overline{C}_l^{do}, \overline{C}_g^{vo}$	dissolved oil and volatized oil equilibrium concentrations ($M\ L^{-3}$)
C_l^{do}, C_g^{vo}	oil concentrations in the aqueous and gas phases ($M\ L^3$)
M_l, M_o, M_g	water, oil and gas molecular weights (M)
τ_l, τ_g	aqueous and gas phase tortuosity (-)
D_l^{do}, D_g^{vo}	dissolved oil and volatilized oil diffusion coefficients ($M^2\ T^{-1}$)
χ_l^{do}, χ_g^{vo}	dissolved oil aqueous mole fraction, volatilized oil gas mole fraction (-)
ω_s^o, ω_l^{do}, ω_g^{vo}	sorbed, dissolved, and volatilized oil mass fraction in the solid, aqueous, and gas phase, respectively (-)

For convenience, k_v is used for $k_{n,g}^{vo}$ and k_{dis} for $k_{n,l}^{do}$ hereafter. Both the kinetic volatilization and the kinetic dissolution are simulated using the k_v and k_{dis} relationships as given below.

3.2.2 Kinetic Volatilization Models

A modified Sherwood number for volatilization process, S_{h0}^v, has been used in the literature to characterize volatilization of entrapped NAPL in porous media

$$S_{h0}^v = \frac{k_v d_{50}^2}{D_{mg}} \tag{3.4}$$

where D_{mg} is the diffusion coefficient (L^2/T) of specific contaminant in the gas phase and d_{50} is the mean particle size (L).

Gas Peclet number P_e^g is the ratio of gas advective mixing to molecular diffusion:

$$P_e^g = \frac{v_g d_{50}}{D_{mg}} \tag{3.5}$$

where, and v_g is the pore-gas velocity of the advective gas phase (L/T). Multiple stepwise regression analysis is usually conducted to determine the best fit using the log-linearized form of the Gilliland–Sherwood correlation as shown below:

$$\log(S_{h0}^{v}) = b_0 + b_1 \log(P_e^g) + b_2 \log(d_0) \text{ or}$$
$$S_{h0}^{v} = 10^{b_0} (P_e^g)^{b_1} d_0^{b_2} \tag{3.6}$$

where b_0, b_1, and b_2 are constants, d_0 is the normalized grain size:

$$d_0 = d_{50} / d_m \tag{3.7}$$

where d_m = 0.05 cm. Substituting Eqs. (3.5) and (3.7) into (3.4) and rearranging produces

$$k_v = 10^{b_0} v_g^{b_1} d_{50}^{b_1+b_2-2} D_{mg}^{1-b_1} d_m^{-b_2} \tag{3.8}$$

It is noted that Eq. (3.8) is applicable to the case that $v_g > 0$ because, if $v_g = 0$, then $k_v = 0$, which is physically incorrect due to the existence of molecular diffusion of oil from NAPL to gas. Hence, when implementing the kinetic k_v models, a minimum v_g is used arbitrarily.

3.2.2.1 The Wilkins et al. (1995) Model

Wilkins et al. (1995, Eq. 15) developed the following relationship based on experiment data:

$$S_{h0}^{v} = 10^{-2.79} (P_e^g)^{0.62} d_0^{1.82}, \; 0.02 < P_e < 20 \tag{3.9}$$

The NAPL-gas first-order mass transfer coefficient can be determined by (Wilkins et al. 1995, Eq. 17)

$$k_v = 10^{-0.42} v_g^{0.62} D_{mg}^{0.38} d_{50}^{0.44}, \text{ units for length: cm} \tag{3.10}$$

The model was able to represent the NAPL-vapor phase mass transfer data over three-order of magnitude of the gas Peclet number range (between 0.02 and 20 based on the Fig. 4 of Wilkins et al. 1995).

3.2.2.2 The van der Ham and Brouwers (1998) Model

van der Ham and Brouwers (1998, Eq. 22) developed a relationship:

$$S_{h0}^{v} = 10^{-3.03} (P_e^g)^{0.88} d_0^{1.82}, \; 5 < P_e < 60 \tag{3.11}$$

where d_0 was defined in the same way as Eq.(3.7) According to Eq. (3.8),

$$k_v = 10^{-0.662} v_g^{0.88} D_{mg}^{0.12} d_{50}^{0.7}, \text{ units for length: cm} \tag{3.12}$$

After a comparison of measurements and predictions, van der Ham and Brouwers (1998) found that Eq. (3.12) is better for $2 < P_e^g < 60$. They recommended the Wilkins et al. (1995) model for $P_e^g < 2$.

3.2.2.3 The Yoon et al. (2002) Model

Yoon et al. (2002, Eq. 7) developed the relationships:

$$S_{h0}^v = 10^{-2.77}(P_e^g)^{0.68} d_0^{1.68} \tag{3.13}$$

$$k_v = 10^{-0.58} v_g^{0.68} D_{mg}^{0.32} d_{50}^{0.36}, \text{ units for length: cm} \tag{3.14}$$

Equation (3.14) is the same as Eq. (8) of Yoon et al. (2002) except the later mistyped 0.36 as 0.34. Yoon et al. (2002) did not state clearly the P_e^g range in their experiments.

3.2.2.4 The Constant k_v Model

Because the kinetic k_v models described above may not provide satisfactory prediction in all cases, a constant k_v model is included in the modified STOMP-WOA. In this case, the k_v for a soil/rock type is a constant all the time and is independent of any system conditions.

3.2.2.5 Comparison of the Kinetic Volatilization Models

A comparison of the three non-constant k_v models as a function of P_e^g is shown in Figure 3.1 for three soils with different mean particle size. The predicted k_v values from the three models have the same trend, although those from the Wilkins et al. (1995) and the Yoon et al. (2002) are most similar.

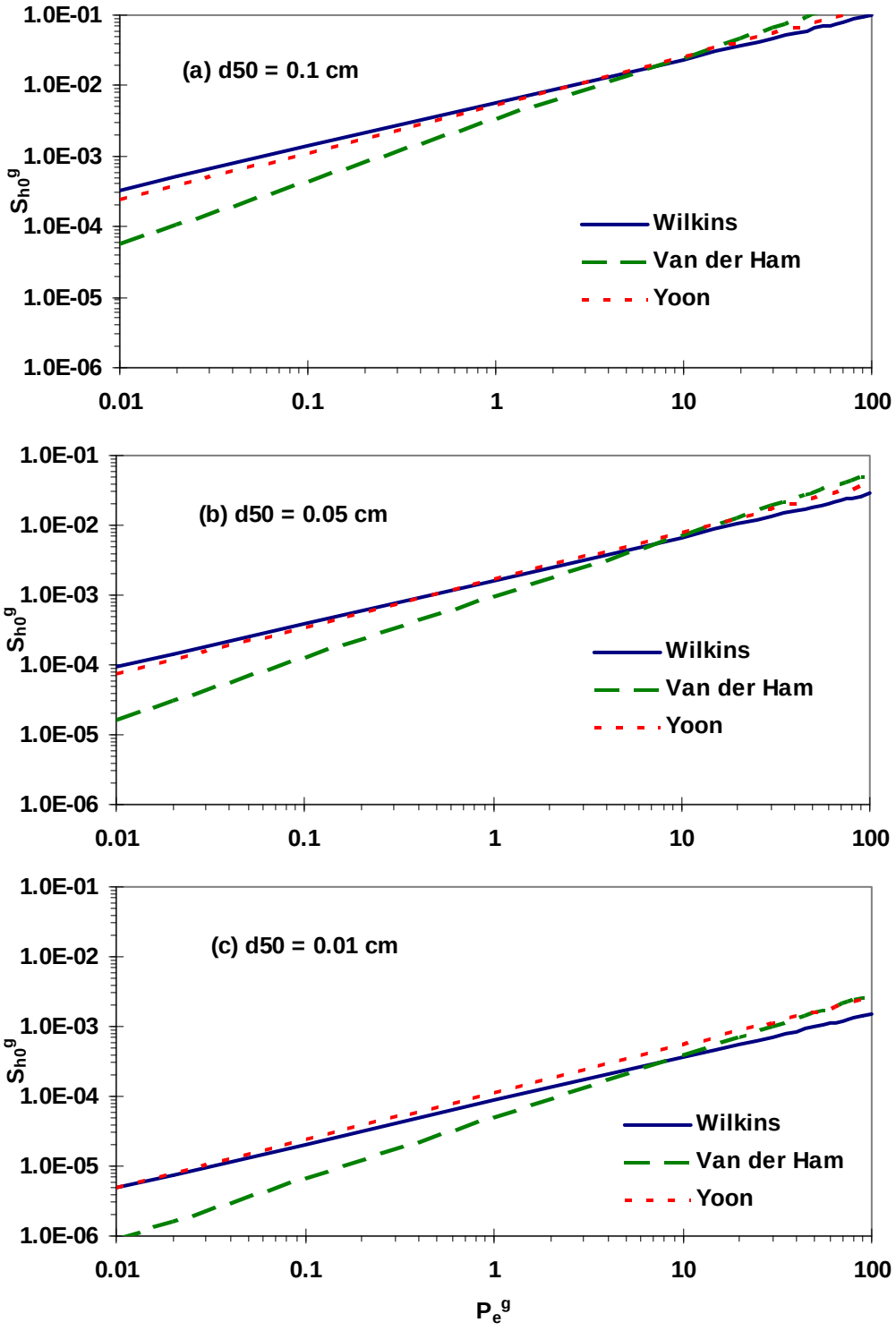

Figure 3.1. Comparison of the Wilkins et al. (1995), the van der Ham and Brouwers (1998), and the Yoon et al. (2002) Models for $0.01 \leq P_e^g \leq 100$ for Three Soils of Different Mean Particle Size.

3.2.3 Kinetic Dissolution Models

The modified Sherwood number , S_{h0}^{dis} , for dissolution of entrapped NAPL in porous media is defined as

$$S_{h0}^{dis} = \frac{k_{dis} d_{50}^2}{D_{ml}} \tag{3.15}$$

where D_{ml} is the diffusion coefficient (L^2/T) of specific contaminant in the aqueous phase.

The Schmidt Number, S_c, is defined as

$$S_c = \frac{\mu_l}{\rho_l D_{ml}} \tag{3.16}$$

The Reynolds number, R_e, for the aqueous phase is defined as:

$$R_e = \frac{q_l \rho_l d_{50}}{\mu_l} \tag{3.17}$$

where q_l is Darcy velocity (L/T). The Reynolds number, R_e', may also be defined based on pore-water velocity v_l (L/T):

$$R_e' = \frac{v_l \rho_l d_{50}}{\mu_l} \tag{3.18}$$

There are numerous empirical models available in the literature to estimate the NAPL dissolution coefficient. Miller et al. (1990) summarized the models developed by then. The NAPL dissolution models developed after 1990 are summarized in Table 3.1. A few observations are:

- Models #1, #5, and #10 used R_e', while other used R_e.
- In all the models except #7, S_h^{dis} is dependent on the NAPL saturation (or content).
- In all the models, $S_h^{dis} = 0$ when the aqueous velocity $v_l = 0$ (v_l is used to calculate R_e as given in Eq. (3.17).
- In modes #6 to #10, S_h^{dis} is also dependent on either medium uniformity or distance.
- Models #11 and #12 were developed based on model #7 (Powers et al. 1994).

Table 3.1. NAPL-Aqueous Phase Mass Transfer Correlations Developed after 1990

No.	Model Source	Correlation	Valid Range	Notes
1	Miller et al. (1990)	$S_{h0}^{dis} = 12 S_c^{0.5} R_e^{'0.75} \theta_n^{0.60}$ $(S_{h0}^{dis} = 425 R_e^{'0.75} \theta_n^{0.60})$	$0.016 < \theta_n < 0.07$; $0.0015 < R_e^{'} < 0.1$	Eq. (27) (See Imhoff et al. 1993, Table 1)
2	Parker et al. (1991)	$S_{h0}^{dis} = 1240(1-\theta_n) R_e^{0.75} \theta_n^{0.60}$	$0.02 < \theta_n < 0.03$; $0.1 < R_e < 0.2$	See Imhoff et al. (1994, Table 5)
3	Imhoff et al. (1994a)	$S_{h0}^{dis} = 150 R_e^{0.87} \theta_n^{0.79}$	$0 \le \theta_n \le 0.04$ $0.0012 \le R_e \le 0.021$	Table 4, Model 1
4	Imhoff et al. (1994a)	$S_{h0}^{dis} = 3.7 R_e^{0.82} \theta_n^{0.58}$	$1.4 \le R_e \le 180$	Table 4, Model 2
5	Nambi and Powers (2003)	$S_{h0}^{dis} = 37.2 R_e^{'0.61} S_n^{1.24}$	$0.01 < S_n < 0.35$; $(0.0048 < \theta_n < 0.168)$; $0.018 < R_e^{'} < 0.134$	Eq. 6 and Table 3
6	Powers et al. (1992)	$S_{h0}^{dis} = 57.7 R_e^{0.61} d_{50}^{0.64} U^{0.41}$	$0.01 < R_e < 1$	Eq. (10)
7	Powers et al. (1994)	$^{lis}_{0} = 4.13 R_e^{0.598} (d_{50}/0.05)^{0.598} U^{0.369} (\theta_n/\theta_{ni})^{\beta}$	$0.0003 < \theta_n < 0.065$; $0.052 < Re < 0.08$; $1.19 < U < 3.33$	Eq. (5)
8	Imhoff et al. (1994a)	$S_{h0}^{dis} = 150 R_e^{0.77} \theta_n^{0.83} [1 - \exp(-89 d_{50}/x)]$	$0 \le \theta_n \le 0.04$ $0.0012 \le R_e \le 0.021$	Table 4, Model 3
9	Imhoff et al. (1994a)	$S_{h0}^{dis} = 340 R_e^{0.71} \theta_n^{0.87} (d_{50}/x)^{-0.31}$	$1.4 \le R_e \le 180$	Table 4, Model 4
1	Saba and Illangasekare (2000)	$S_{h0}^{dis} = 11.34 R_e^{'0.2767} S_c^{0.33} (\theta_n d_{50}/\tau L)^{1.037}$	$0.0005 < R_e^{'} < 0.0075$; $0.25 < v_l < 3.0$ m/d	Eq. (6)
1	Brusseau et al. (2002)	$k_{dis} = k_{dis0} [R_e(t)/R_{e0}]^{0.598} (\theta_n/\theta_{ni})^{\beta}$	$0.020 \le S_n \le 0.111$	Eq. (5), base on Powers et al. (1994)
1	Clement et al. (2004)	$k_{dis} = k_{dis0} (\theta_n/\theta_{n0})^{\beta}$	-	Eq. (4), base on Powers et al. (1994)

$\beta = 0.518+0.114(d_{50}/d_m)+0.10U$ (Brusseau et al. 2002, p1035; Clement et al. 2004, Eq. A.4);
U: uniformity index; θ_{ni}: initial NAPL content; x: distance from the dissolution cell entrance;
L: length of the contaminated soil block in the flow direction;
τ: the tortuosity of the porous medium; k_{dis0} is the k_{dis} value at θ_{n0}.

The Nambi and Powers (2003) model was selected to simulate the NAPL kinetic dissolution process in the modified STOMP-WOA. Like many of the other models, the Nambi and Powers (2003) model predicts a zero of k_{dis} when the aqueous phase is not moving ($R_e = 0$). Hence, a minimum value of v_l was arbitrarily applied. Nambi and Powers (2003) employed a stepwise regression technique to systematically evaluate optimum combinations of the parameters for the phenomenological model in order to obtain the best fit to the experimental data. The first regression was done with only one variable, NAPL saturation. The stepwise regression procedure involved the stepwise addition of the other individual parameters. After each addition of a parameter, the new model was assessed for its quality of fit to the data and its adequacy by comparing the coefficient of determination, R^2, among correlations and by performing an F test. Based these results, the regression presented as model #5 in Table 3.1 is their simplest correlation that adequately described the NAPL dissolution within the coarse sand lens in their two-dimensional experimental system.

3.3 STOMP Modifications

3.3.1 Summary of Modification

1. Modifications were incorporated into the STOMP-WOA mode to include models for kinetic volatilization and dissolution. A local equilibrium approach to describe NAPL volatilization and dissolution previously available in this mode can also be selected by the user.
2. The user can select one of the following four models to describe kinetic volatilization of NAPL:
    a. the Wilkins et al. (1995) model
    b. the van der Ham and Brouwers (1998) model
    c. the Yoon et al. (2002) model
    d. constant volatilization coefficient
3. The Nambi and Powers (2003) model is used to describe kinetic dissolution of NAPL regardless of the selection of the kinetic volatilization model.

3.3.2 Assumptions

1. Because the kinetic NAPL volatilization and dissolution processes occur simultaneously, it is assumed that the oil vapor pressure and dissolved oil concentration are always in equilibrium as defined by the Henry's Law constant.
2. The kinetic models produce a zero value for either the volatilization or dissolution coefficient when the gas or aqueous velocity equals zero. However, in real systems dissolution and volatilization can still occur due to diffusion under this condition. The code imposes a value of 10^{-10} m s^{-1} as the minimum gas or aqueous velocity of v_g or v_l to avoid conditions that would produce a zero value for the kinetic volatilization or dissolution coefficient. Users should consider use of the equilibrium volatilization and dissolution models for systems with zero or near zero gas or aqueous velocity.

3.3.3 Summary of Subroutine Modification

The program stomp5.F was modified.

1. The following new subroutines were developed
   a. kv5: computes kinetic volatilization rate (M T^{-1}), where mass transfer of oil between phases is defined as positive from NAPL-oil to the volatilized-oil or the dissolved-oil.
   b. av5: computes average gas and aqueous velocities for the kinetic option.
2. Calls to the new subroutines were added appropriately
3. Selective statements were added to distinguish the kinetic mass transfer from equilibrium mass transfer

3.3.4 Input Modification

The key words "w/ Kinetic Volatilization" are used after "Water-Oil-Air" in the "Solution Control Card" to evoke the kinetic volatilization and dissolution of NAPL. The existing code already has the capability to calculate the oil diffusivity in the gas (D_{mg}) or aqueous (D_{ml}) phase and the required data for their estimations are inputted in the "Solution Control Card". Additional input data (d_{50} or k_v, model name) for the kinetic option are needed in the "Oil Transport" card. The input format, following the convention in the STOMP users' manual, is given below:

if: Operational Model = {STOMP-WOA}
  Rock/Soil Name[a], Longitudinal Dispersivity[b], Units[c] (m), Transverse Dispersivity[d], Units[e] (m), Constant K_d[f], Units[g] (m^3/kg),
  format: Char[a], Real[b], Char[c], Real[d], Char[e], Real[f], Char[g],
elseif: Operational Model = {STOMP-WOA w/ Kinetic Volatilization}
  Rock/Soil Name[a], Longitudinal Dispersivity[b], Units[c] (m), Transverse Dispersivity[d], Units[e] (m), K_d[f], Units[g] (m^3/kg),
  if: Kinetic model = {Winkins | Yoon | van der Ham and Brouwers}
    d_{50}[h], Units[i] (m),
  else if: Kinetic model = {Constant}
    k_v[h], Units[i] (1/s),
  endif:
Model name[j],
  format: Char[a], Real[b], Char[c], Real[d], Char[e], Real[f], Char[g], Real[h], Char[i],
  format: Char[j],
endif:

The superscripts of small case letters are used to relate variable names and their types and input sequence in the STOMP input file. Items separated by a "|" symbol are selective.

3.4 Code Evaluation

A 0.3×0.3×0.3 m domain was discretized into 3×3×3 = 27 nodes. Multiple simulations as described below were conducted to evaluate the modified STOMP-WOA. There were 17 test cases in total, a base case and 16 variations (Table 3.2). For the base case (Case 1), about 140 g carbon tetrachloride existed initially at the center of the cubic domain that contained a sandy soil; clean gas moved into the domain under a pressure gradient of 100 Pa/m; during the gas movement, NAPL was volatilized and the oil vapor

was taken out of the domain with the moving gas. The complete listing of a STOMP input file is given in Appendix A for the base case scenario when the Wilkins et al. (1995) model was used. For cases 2 through 17, one variable was varied from the base case (Case 1) except where specifically noted.

Each case except Case 2 contains 4 simulation scenarios (Table 3.3), which correspond to the equilibrium volatilization model (EQ) and the three kinetic volatilization models [i.e., the Wilkins et al. (1995) model, WI, the van der Ham and Brouwers (1998), VB, and the Yoon et al. (2002) models, YO]. Case 2 contains 3 simulation scenarios with the constant volatilization coefficient model with k_v being 0.0001 (CO_1), 0.001 (CO_2), and 0.01 (CO_3) s^{-1}, respectively.

Two types of evaluations were carried out:

1. Quantitative evaluations:
   a. the STOMP code was compiled with the debug mode and the volatilization and dissolution coefficients were tracked and compared with the analytically calculated values for the four scenarios of Case 1 (base case).
   b. mass balance was calculated for the scenarios of Cases 1 and 2.
2. Qualitative evaluations: different physical processes (NAPL volatilization and/or dissolution) and different physical conditions (particle size, boundary condition type, source type) were investigated. The results were evaluated by comparing the observed to the expected trends due to the parameter change.

3.5 Test Results

Test results for the quantitative and qualitative evaluations are described in the following sections.

3.5.1 Quantitative Evaluation

The kinetic volatilization and dissolution coefficients at the initial times of the simulations were analytically calculated with MathCad® 12[1] and numerically with the modified STOMP code for the four scenarios of Case 1 (base case). The comparisons of the results are summarized in Table 3.4. The differences between the analytical and numerical results were no more than 0.93%. The small differences were caused by the approximation of the constants in the kinetic volatilization or dissolution models.

The error of oil mass balance at the end of a simulation was calculated with the following equation:

$$E_{ba}\,(\%) = 100(M_t - M_{in} - M_{out})/M_t \qquad (3.19)$$

where $E_{ba}(\%)$ is mass balance error in percent, M_t is the total oil mass, M_{in} and M_{out} are the oil mass residing in and migrated out of the simulation domain at the end of a simulation, respectively. The oil mass balance for the 4 scenarios of Case 1 (base case) and the 3 scenarios of Case 2 are summarized in Table 3.5. The absolute values of the errors were no more than 1.2 %.

[1] Mathsoft Engineering & Education, Inc., 2004. Cambridge, MA.

Table 3.2. Description of Test Cases for Kinetic Volatilization Model

Case No.	Objective	Description
1	quantitative evaluations; as a base for qualitative evaluations	gas gradient = 100 Pa/m; aqueous gradient = 0; gas moved into the system from left and out from the right; residual NAPL resided at the center part of the domain; d_{50} = 0.02 cm; there were no other sources
2	mass balance evaluations	models with constant k_v
3	effects of d_{50}	d_{50} = 0.002 cm
4		d_{50} = 0.2 cm
5	effects of gas velocity on NAPL volatilization	gas gradient = 20 Pa/m
6		gas gradient = 500 Pa/m
7		gas gradients were 20, 100, and 500 Pa/m for t <0.1 d, 0.1≤ t ≤0.2, and t > 0.2 day, respectively
8		gas gradients were 500, 100, and 20 Pa/m for t <0.03 d, 0.03≤ t ≤0.1, and t > 0.1 day, respectively
9	effects of aqueous velocity on NAPL dissolution	saturated system; aqueous gradient = 500 Pa/m
10		saturated system; aqueous gradient = 1000 Pa/m
11		saturated system; aqueous gradient = 2000 Pa/m
12	effects of a gas source	a gas source of 100 L/d; no gas entering through a boundary
13		a gas source of 1000 L/d; no gas entering through a boundary
14	effects of a water source	a water source of 100 L/d; no gas entering through a boundary
15		a water source of 1000 L/d; no gas entering through a boundary
16	effects of a NAPL source	a NAPL source of 0.2 L/d for 0.25 days
17		a NAPL source of 0.2 L/d for 0.5 days

Table 3.3. Description of Simulation Scenarios

Scenario Name	Model Name	Description
EQ	Equilibrium	Oil partition between phases is always at equilibrium
WI	Wilkins (1995)	Eq. (3.10)
VB	van der Ham and Brouwers (1998)	Eq. (3.12)
YO	Yoon et al. (2002)	Eq. (3.14)

Table 3.4. Kinetic Volatilization and Dissolution Coefficients (s^{-1})

Model	Volatilization or Dissolution Coefficients		
	Analytical	Numerical	Difference
Wilkins (1995)	2.942E-3	2.956E-3	+0.48%
van der Ham and Brouwers (1998)	1.185E-3	1.185E-3	0.00%
Yoon et al. (2002)	3.227E-3	3.257E-3	+0.93%
Nambi and Powers (2003) Model:	3.143E-6	3.142E-6	+0.03%

Table 3.5. Oil Mass Balance at the End of Simulation

			Out of the Domain					
Scenarios	Total (g)	In Domain (g)	Gas Oil West Boundary (g)	Gas Oil East Boundary (g)	Dissolved Oil West Boundary (g)	Dissolved Oil East Boundary (g)	Total Oil (g)	E_{ba}(%)
EQ	1.401E+02	0.000E+00	3.906E-02	1.400E+02	1.083E-06	9.871E-05	1.401E+02	0.000
VB	1.401E+02	5.830E+00	4.111E-02	1.341E+02	7.220E-07	3.249E-05	1.341E+02	-0.072
WI	1.401E+02	0.000E+00	4.237E-02	1.391E+02	7.621E-07	3.721E-05	1.391E+02	-0.666
YO	1.401E+02	0.000E+00	4.269E-02	1.402E+02	7.700E-07	3.791E-05	1.403E+02	0.151
CO_1	1.401E+02	1.247E+02	4.769E-03	1.516E+01	8.346E-08	3.410E-06	1.517E+01	-0.166
CO_2	1.401E+02	0.000E+00	4.231E-02	1.384E+02	7.479E-07	3.456E-05	1.384E+02	-1.205
CO_3	1.401E+02	0.000E+00	3.872E-02	1.388E+02	1.070E-06	9.888E-05	1.389E+02	-0.871

3.5.2 Qualitative Evaluation

3.5.2.1 Kinetic Volatilization Models

The effects of different NAPL volatilization models were examined with the 4 scenarios of Case 1 (base case) and the 3 scenarios of Case 2. As shown in Table 3.4, the Wilkins (1995) and Yoon et al. (2002) models produced similar k_v values (0.0029 vs. 0.0032 s^{-1}), while the van der Ham and Brouwers (1998) model produced a much smaller k_v value (0.0012 s^{-1}). Consequently, under the same conditions, the volatilization process with the van der Ham and Brouwers (1998) model is significantly slower than those with the other two models (Figure 3.2a,b). This is consistent with the findings mentioned in a previous section (Figure 3.1).

User-defined constant k_v values can also be used. This was examined with the 3 constant k_v values (Case 2). As shown by Figure 3.2c and Figure 3.2d, a smaller k_v value corresponds to a slower volatilization process. Because the equilibrium model assumes instantaneous equilibrium, it is the upper bound of the kinetic models. Namely, no kinetic model should produce a volatilization process faster than the equilibrium model. Thus, as k_v increases, the kinetic model should produce results similar to the equilibrium model (e.g., see results for $k_v = 0.01$ s^{-1} in Figure 3.2c, d). Any attempt to increase k_v further will not have any effect on the NAPL volatilization process. These results correctly reflect the NAPL volatilization rate variation.

3.5.2.2 Effects of Mean Particle Diameter on NAPL Volatilization

The effects of the mean particle diameter on NAPL volatilization were investigated with Cases 1, 3 and 4. All the conditions for Cases 3 and 4 were the same as those of Case 1 (base case) except the mean particle diameter. Figure 3.3 shows oil concentration in the gas phase and cumulative gas oil mass migrated out of the domain. As expected, the mean particle diameter had no effect on the equilibrium model, as shown by the time (~0.3 day) that all NAPL was volatilized/dissolved. For the kinetic models, the volatilization process increased with increasing particle diameter; as the particle diameter became larger, the oil concentration in the gas phase was higher and more cumulative gas oil migrated out of the domain. These results are consistent with the effects of particle size on k_v shown by Eqs. (3.10), (3.12), and (3.14).

3.5.2.3 Effects of Gas Velocity on NAPL Volatilization

The effects of gas velocity on NAPL volatilization were investigated with Case 1 (base case) and Cases 5 through 8. All the conditions for Cases 5 through 8 were the same as those of the base case except the gas pressure gradient across the system. As shown in Figure 1.4, the total gas mass volatilized at any given time increased with increasing gas velocity, as expected. The impacts of varying gas velocity on the gas oil concentration near the NAPL source are shown in Figure 3.5. For the equilibrium model, the gas oil concentration was independent of gas velocity as long as NAPL existed; when all the NAPL was volatilized, the gas oil concentration dropped to zero almost instantly. For the kinetic models, the gas oil concentration near the NAPL source was dependent on the gas velocity. As the gas velocity increased, the gas oil concentration decreased due to the time needed for NAPL volatilization (Figure 3.5a through c). When gas velocity varied with time (Figure 3.5d and e), the gas oil concentration also varied with time correspondingly when the kinetic models were used.

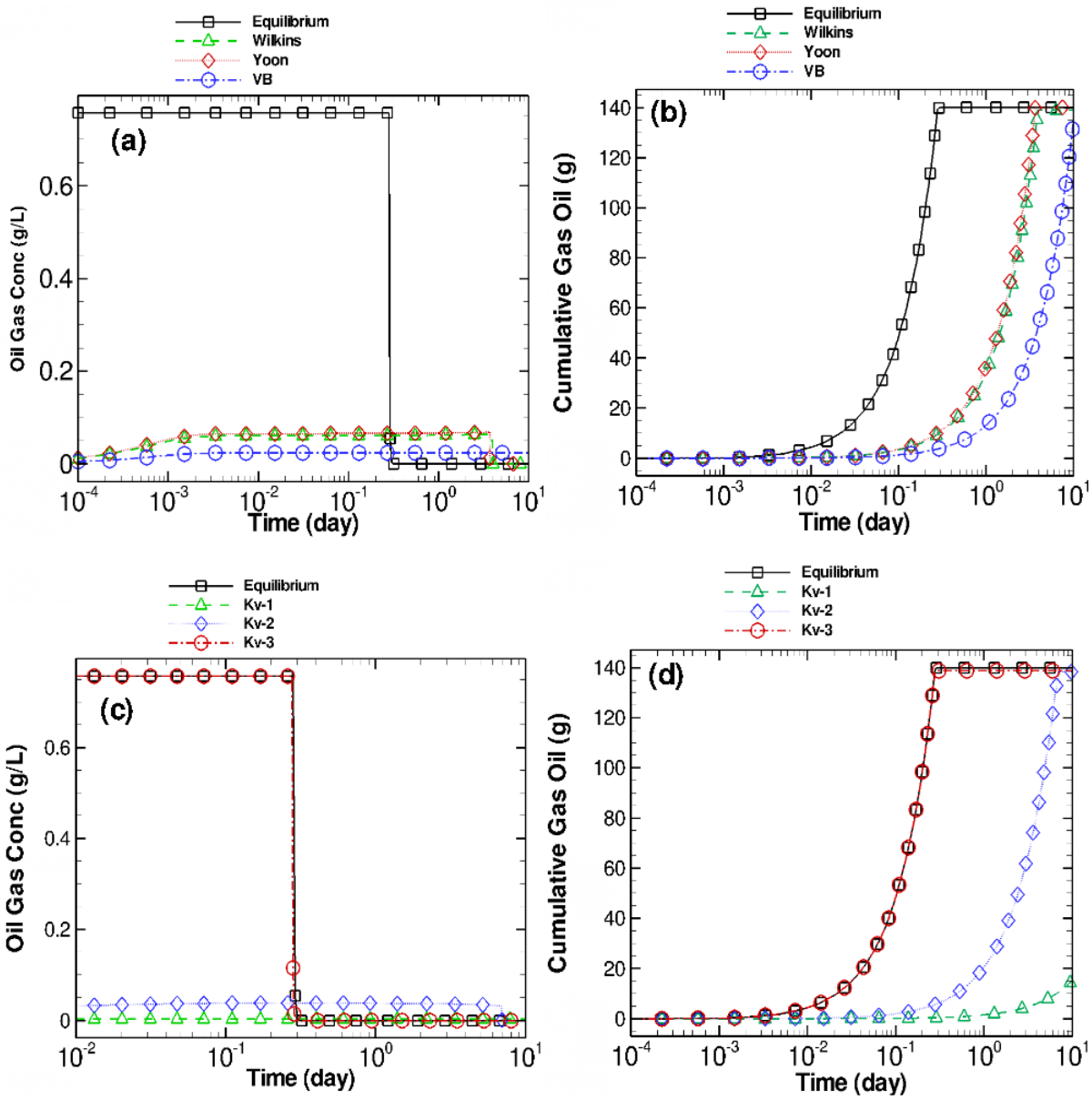

Figure 3.2. (a) and (b) Comparison of the Equilibrium, Wilkins (1995), Yoon et al. (2002), the van der Ham and Brouwers (1998) Models (Case 1); (c) and (d) Comparison of the Equilibrium Model and Those with Constant k_v values, $k_v\_1 = 0.0001\ s^{-1}$, $k_v\_2 = 0.001\ s^{-1}$, and $k_v\_3 = 0.01\ s^{-1}$ (Case 2)

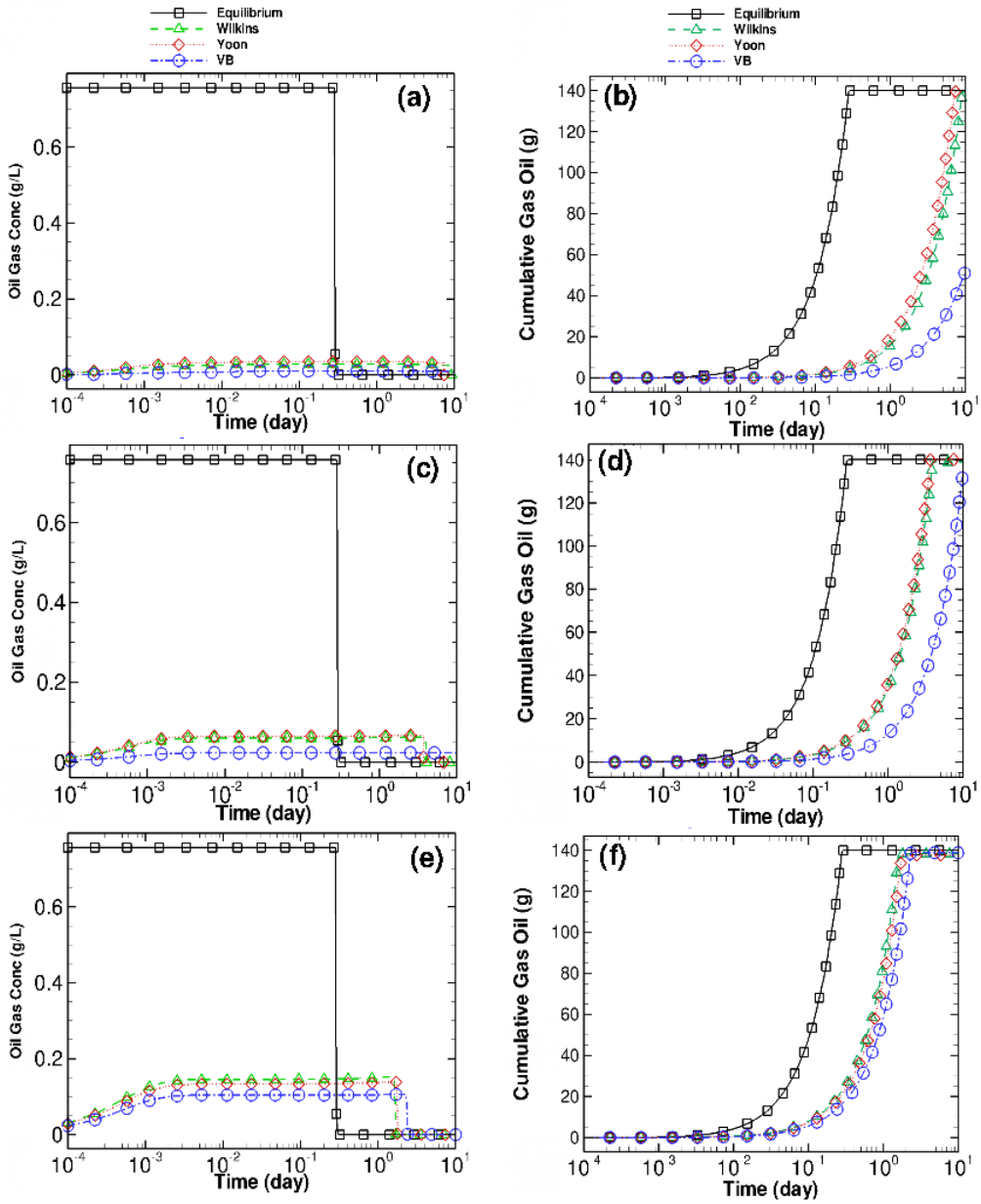

Figure 3.3. Effects of mean particle diameter (d_{50}) on NAPL volatilization. (a) and (b) d_{50} = 0.002 cm (Case 3), (c) and (d) d_{50} = 0.02 cm (Case 1), and (e) and (f) d_{50} = 0.2 cm (Case 4)

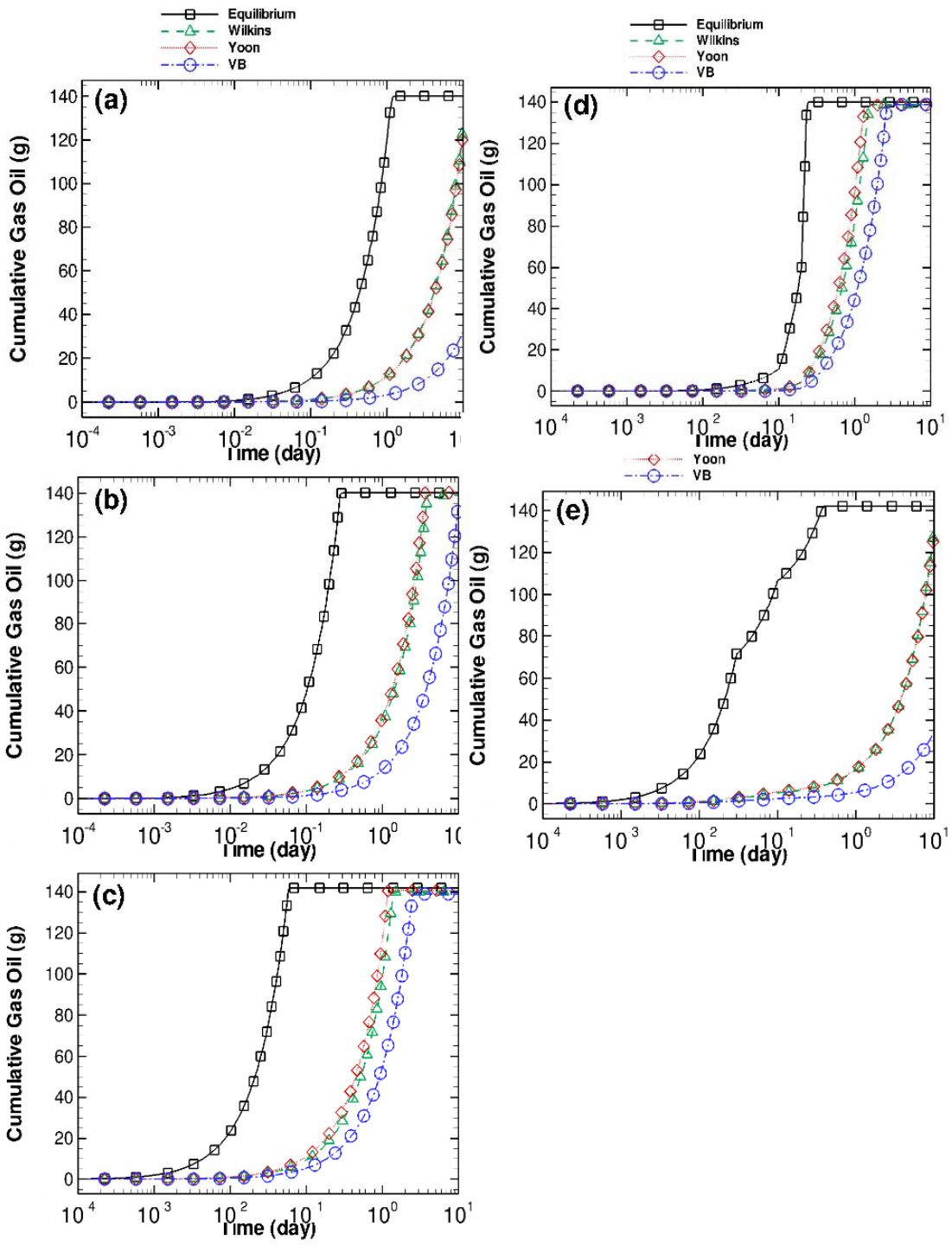

Figure 3.4. Effects of Gas Velocity on the Cumulated Gas Oil Migrated out of the Domain. (a) Gas Pressure Gradient = 20 Pa/m (Case 5); (b) Gas Pressure Gradient = 100 Pa/m (Case 1), (c) Gas Pressure Gradient = 500 Pa/m (Case 6), (d) Gas Pressure Gradient = 20, 100 and 500 Pa/m for t <0.1 d, 0.1≤ t ≤0.2, and t > 0.2 day, Respectively (Case 7), and (e) Gas Pressure Gradient = 500, 100 and 20 Pa/m for t <0.03 d, 0.03≤ t ≤0.1, and t > 0.1 day, Respectively (Case 8)

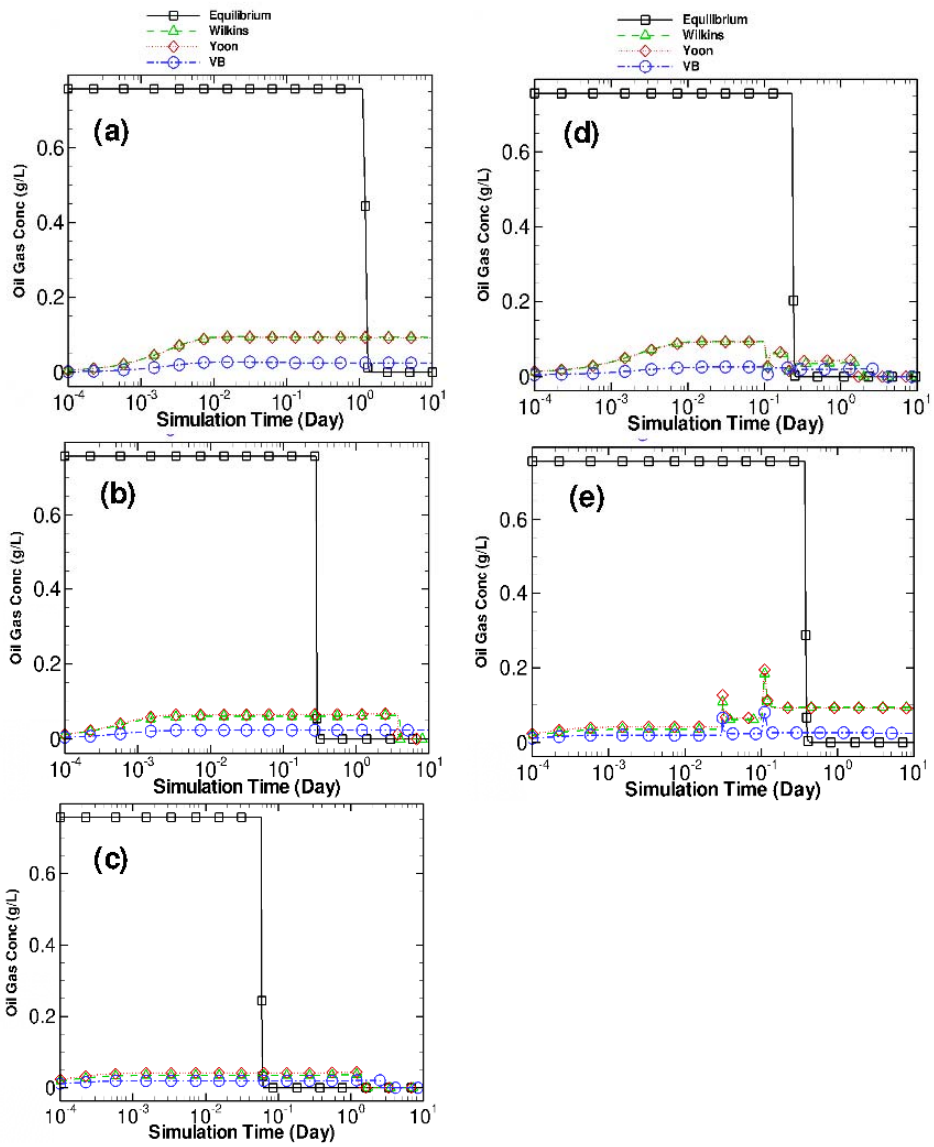

Figure 3.5. Effects of Gas Velocity on the Gas Oil Concentration. (a) Gas Pressure Gradient = 20 Pa/m (Case 5); (b) Gas Pressure Gradient = 100 Pa/m (Case 1), (c) Gas Pressure Gradient = 500 Pa/m (Case 6), (d) Gas Pressure Gradient = 20, 100 and 500 Pa/m for t <0.1 d, 0.1≤ t ≤0.2, and t > 0.2 day, Respectively (Case 7), and (e) Gas Pressure Gradient = 500, 100 and 20 Pa/m for t <0.03 d, 0.03≤ t ≤0.1, and t > 0.1 day, Respectively (Case 8)

3.5.2.4 Effects of Aqueous Phase Velocity on NAPL Dissolution

The effects of aqueous phase velocity on NAPL dissolution were investigated with Cases 9 through 11. All the conditions for Cases 9 through 11 were the same as Case 1 (base case) except that the system was saturated at all times and different aqueous hydraulic gradients were applied to create different aqueous phase velocity. When the hydraulic gradient increased, the time need to completely dissolve all the NAPL was shortened (Figure 3.6) regardless of the model used; as expected, the maximum oil aqueous concentration (C_{max}^{aq}) was unaffected by the aqueous velocity when the equilibrium model was used;

C_{max}^{aq} became smaller when the kinetic models were used. It is noted that, regardless of the kinetic volatilization models, the same kinetic dissolution model (Nambi and Powers, 2003) is applied.

3.5.2.5 Effects of a Gas Source Rate on NAPL Volatilization

Two different gas source rate were used to show the effect of the gas source rate on NAPL volatilization (Cases 12 and 13). All the conditions were the same as Case 1 (base case) except that 1) there was no gas entering into the system through any boundaries and 2) a gas source was imposed. When the gas release rate increased, the maximum oil gas concentration (C_{max}^{gas}) were unchanged when the equilibrium model was used (Figure 3.7a, c); C_{max}^{gas} became smaller when the kinetic models were used (Figure 3.7a, c); the time needed to completely volatilize all the NAPL was shortened regardless of the model used (Figure 3.7b, d).

3.5.2.6 Effects of a Water Source Rate on NAPL Dissolution

Two different water source rates were used to show the effects of the water source rate on NAPL dissolution. All the conditions were the same as Case 1 (base case) except that 1) there was no gas entering into the system through any boundaries and 2) a water source was imposed. The oil aqueous concentration and the cumulative dissolved oil mass migrated out of the domain are shown in Figure 3.8. When the aqueous source release rate increased, the maximum oil aqueous concentration (C_{max}^{aq}) was unaffected by the aqueous source release rate when the equilibrium model was used but was smaller when the kinetic model were used; the time need to completely dissolve/volatilize all the NAPL was shortened regardless of the model used.

3.5.2.7 Volatilization/Dissolution of a NAPL Source

Two different NAPL source rates were tested to show the effects of the NAPL source rate on NAPL volatilization. All the conditions were the same as Case 1 (base case) except that there was no NAPL in the domain at the beginning of the simulations and a NAPL source was imposed. Figure 3.9 shows the volatilization and dissolution of two NAPL sources of different release duration. As the release duration increased, it took longer time to volatilize and dissolve all the NAPL.

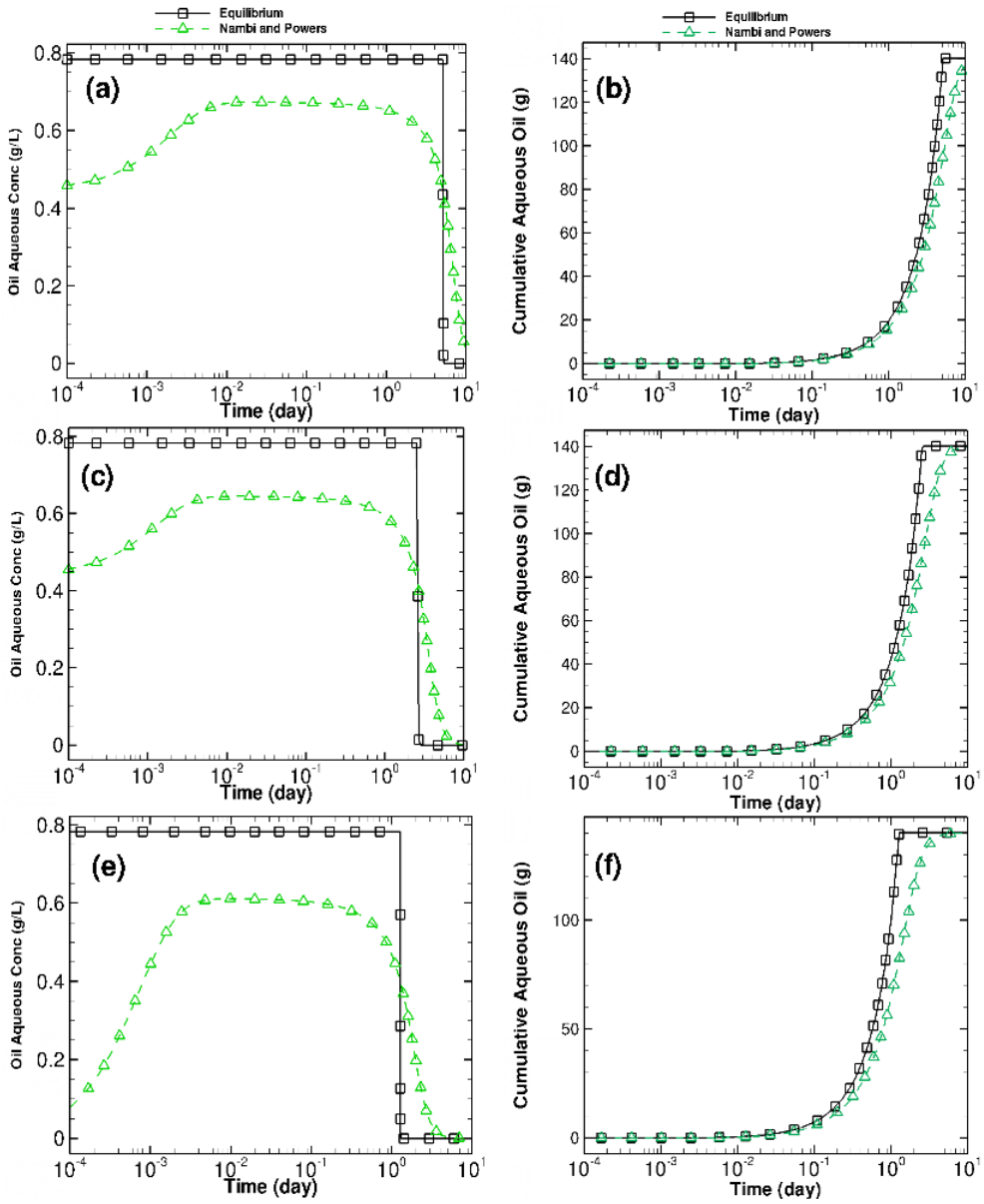

Figure 3.6. Effects of Aqueous Velocity on the Aqueous Oil Concentration. Aqueous Hydraulic Gradients Were (a) and (b) 500 Pa/m (Case 9), (c) and (d) 1000 Pa/m (Case 10), and (e) and (f) 2000 Pa/m (Case 11)

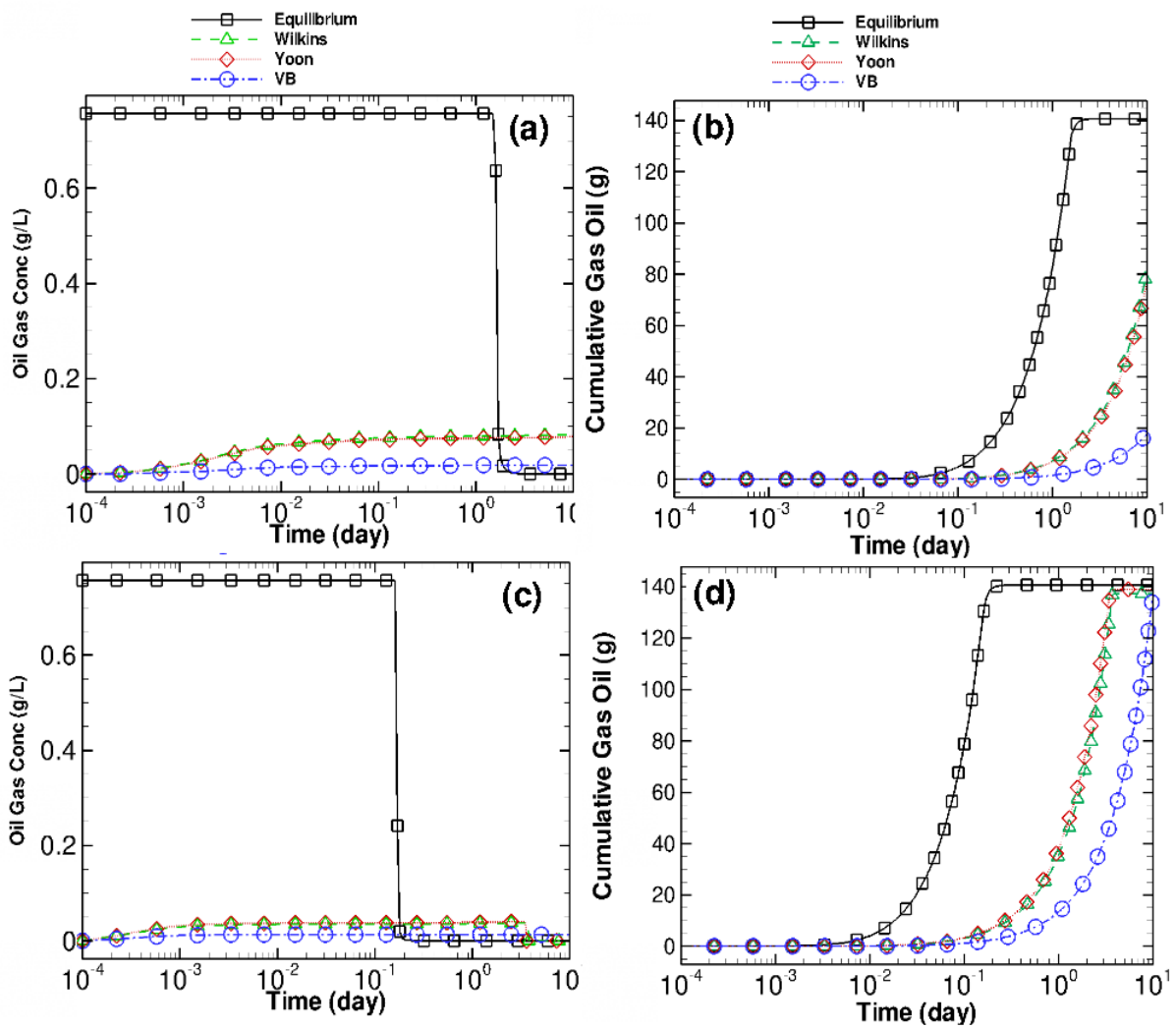

Figure 3.7. Effects of a Gas Source on NAPL Volatilization. Gas Source Release Rate: (a) and (b) 100 L/d (Case 12); and (c) and (d) 1000 L/d (Case 13)

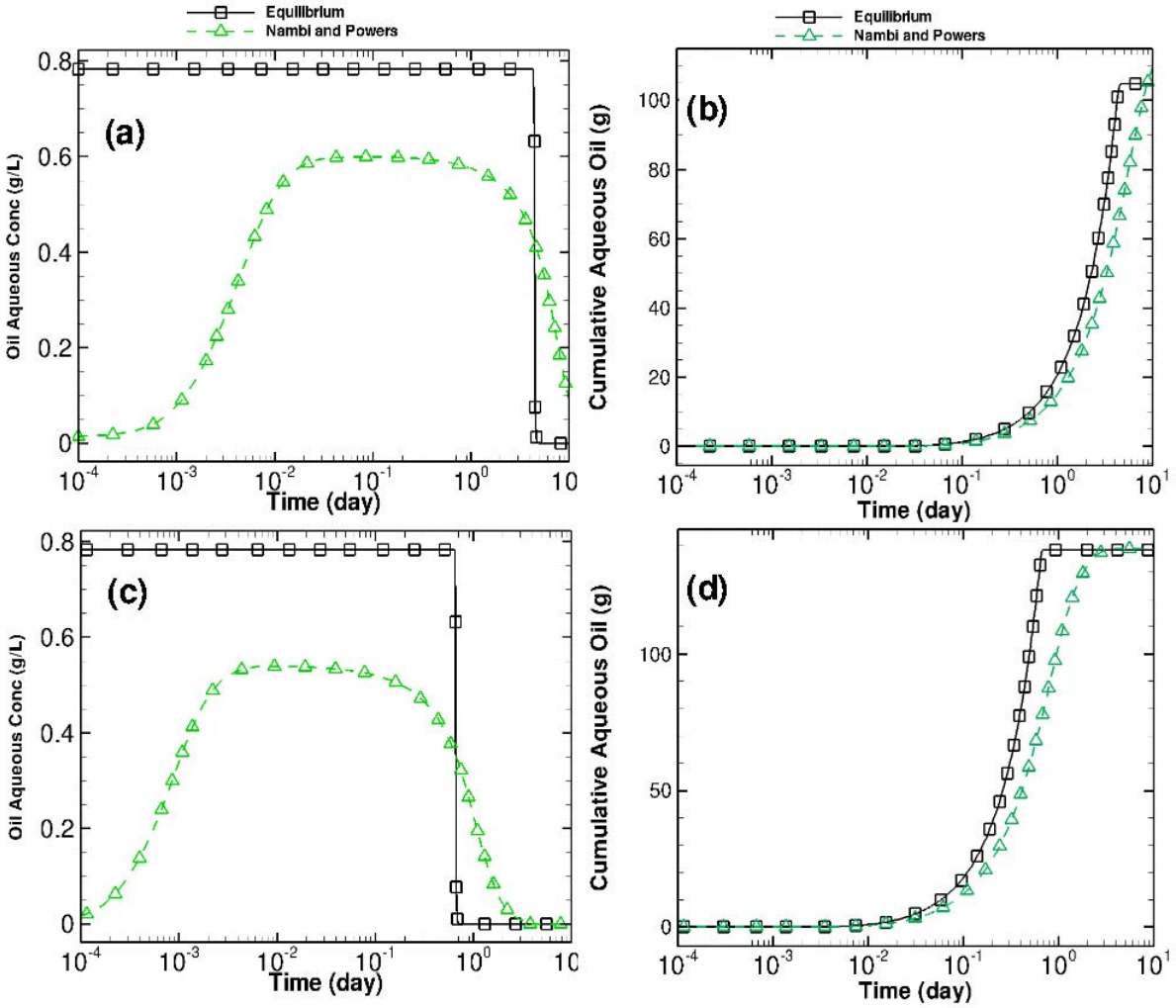

Figure 3.8. Effects of an Aqueous Source on NAPL Dissolution. Aqueous Source Release Rates: (a) and (b) 100 L/d (Case 14) and (c) and (d) 1000 L/d (Case 15)

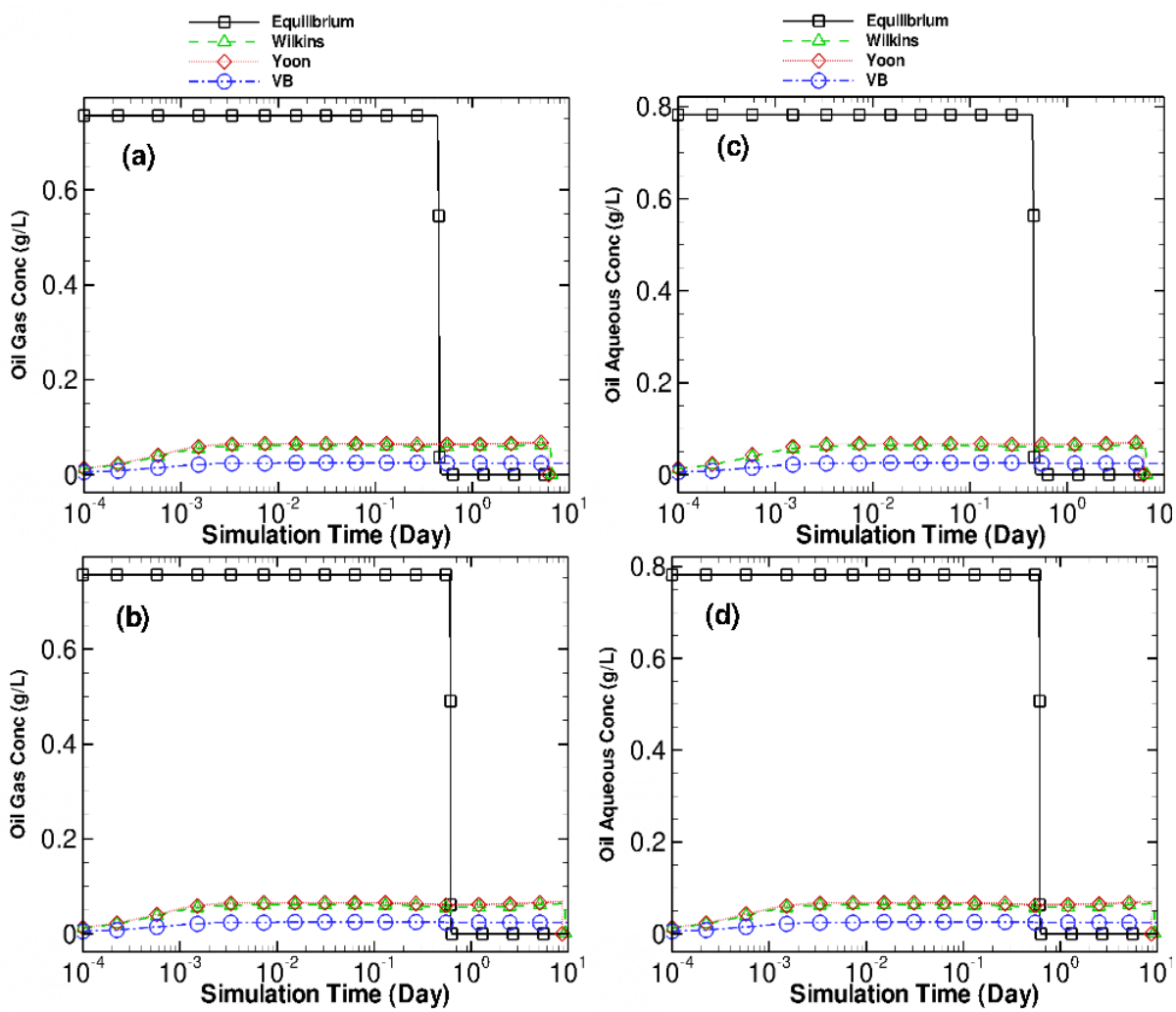

Figure 3.9. Volatilization and Dissolution of a NAPL Source. NAPL Source Strength and Duration: (a) and (c) 0.2 L/d for 0.25 d (Case 16), and (b) and (d) 0.2 L/d for 0.5 d (Case 17)

3.5.3 Test Summary

The above test results show that the kinetic volatilization and dissolution models behave as intended and can adequately describe the physical processes of NAPL kinetic volatilization and dissolution.

4.0 Multicomponent NAPL Formulation

4.1 Computation of Multicomponent Parameter Values

The modifications to the STOMP simulator primarily encompass computation of fluid and gas property values of mixtures. The fluid and gas properties of interest are density, viscosity, and solubility. This section provides an overview of the formulae used in STOMP simulator to compute the average property values. The following variables are used:

χ_{γ}^{j} mole fraction of component *j* in phase γ

μ_{a}^{j} aqueous kinematic viscosity of component j (Pa s)

μ_{g}^{j} vapor kinematic viscosity of component j (Pa s)

μ_{o}^{i} liquid kinematic viscosity of oil component i (Pa s)

Φ_{g}^{jk} vapor binary interaction parameter for component pair *jk*

ρ_{g}^{j} component vapor density of component j (kg/m^3)

ρ_{l} liquid density of water (kg/m^3)

ρ_{sat}^{j} saturated liquid density of oil, (kg/m^3)

$\overline{\rho}_{sat}^{j}$ reference saturated liquid density of component j, (kg/m^3)

ω_{p}^{j} Pitzer acentric factor for component j

A function constant

a function constant

h Hawkinson-Brobst-Thomson liquid density function constants

M molecular weight of component *j* , kg/kgmol

NC total number of NAPL components

P_{c}^{j} critical pressure of component j, Pa

P_{r}^{j} reduced pressure of component j, Pa

P_{sat}^{j} saturated vapor pressure of oil, Pa

R^j universal gas constant of component j, J/kg K

T temperature, K

T_{c}^{j} critical temperature of component j, K

T_{r}^{j} reduced temperature of component j, K

V_{c}^{j} critical specific volume of component j, m^3/kg

Z reduced temperature and pressure factor

Z_{RA}^{j} Racket compressibility factor of component j

4.1.1 Aqueous-Phase Density

In STOMP, low solubility is assumed in the aqueous phase, and density is independent of dissolved component concentrations, aqueous-phase density can be computed as a function of temperature and pressure using the steam table formulations [ASME 1967], given as

$$\rho_l = v_c^w \left\{ \begin{array}{l} A_{11} a_5 Z^{-5/17} + A_{12} + A_{13} T_r^w + A_{14} \left(T_r^w\right)^2 + A_{15} \left(a_6 - T_r^w\right)^{10} \\ + A_{16} \left(a_7 + \left(T_r^w\right)^{19}\right)^{-1} - \left(a_8 + \left(T_r^w\right)^{-11}\right)^{-1} \left(A_{17} + 2A_{18} P_r^w + 3A_{19} \left(P_r^w\right)^2\right) \\ - A_{20} \left(T_r^w\right)^{18} \left(a_9 + \left(T_r^w\right)^2\right) \left(-3\left(a_{10} + P_r^w\right)^{-4} + a_{11}\right) \\ + 3A_{21} \left(a_{12} - T_r^w\right) \left(P_r^w\right)^2 + 4A_{22} \left(T_r^w\right)^{-20} \left(P_r^w\right)^3 \end{array} \right\}^{-1} \tag{4.1}$$

where

$$Z = Y + \left(a_3 Y^2 - 2a_4 T_r^w + 2a_5 P_r^w\right)^{1/2}$$

$$Y = 1 - a_1 \left(T_r^w\right)^2 - a_2 \left(T_r^w\right)^{-6}$$

Numerical values of the constants are listed in Appendix A in White and Oostrom (2000).

4.1.2 NAPL-Phase Density

Liquid oil density for saturated conditions is computed as a function of temperature using the Modified Rackett method [Reid et al. 1987], given as

$$\rho_{sat}^o = \left\{ \left[\frac{R^o T_c^o}{P_c^o} \right] \left(Z_{RA}^o\right)^{\left[1+\left(1-T_r^o\right)^{2/7}\right]} \right\}^{-1} \tag{4.2}$$

where

$$T_r^o = \frac{T}{T_c^o}$$

$$P_r^o = \frac{P}{P_c^o}$$

$$Z_{RA}^o = 0.29056 - 0.08775\omega_P^o$$

If an experimental value for liquid density is available, then the recommended form of the Rackett function is given as

$$\rho_{sat}^o = \left\{ \left[\frac{1}{\overline{\rho}_{sat}^o} \right] \left(Z_{RA}^o\right)^{\left[\left(1-T_r^o\right)^{2/7} - \left(1-\overline{T}_r^o\right)^{2/7}\right]} \right\}^{-1} \tag{4.3}$$

A correction for compressed conditions is made following the Hankinson-Brobst-Thompson (HBT) technique [Reid et al. 1987], according to

$$\rho_n^o = \frac{\rho_{sat}^o}{\left[1 - h_3 \ln\left(\frac{h_9 + P}{h_9 + P_{sat}^o}\right)\right]} \tag{4.4}$$

where

$$h_9 = P_c^o\left[-1 + h\right]$$

Definitions and numerical values for the *h* coefficients are found in White and Oostrom (2000).

Compositional NAPL contains a mixture of liquid-oil components. NAPL-phase density is computed as a function of the pure component liquid densities and molar concentrations in the NAPL phase according to

$$\rho_n = \sum_j^o \chi_n^j \rho_n^j \tag{4.5}$$

Alternatively, mixing rules for the Rackett equation have been published [Reid et al.1987] which define the critical pressure, critical temperature, and critical compressibility for a liquid mixtures. NAPL-phase density for a compositional NAPL can be computed as a function of temperature and pressure using the Modified Rackett and HBT methods by substituting the mixture critical properties for the component critical properties.

4.1.3 Gas-Phase Density

Component vapor densities can be computed using the ideal gas law given as

$$\rho_g^j = \frac{P_g^j}{R^j T}, \quad for\ j = w, a, o \tag{4.6}$$

For single component NAPLs, or for multiple component NAPLs at atmospheric pressure, the ideal gas law is roughly accurate for computing the oil vapor density. When these conditions are violated, this equation becomes increasingly inaccurate. The Peng-Robinson equation (1976) was developed to be applicable to calculations of fluid properties in natural gas processes. The STOMP simulator implements the Peng-Robinson formulation to iteratively calculate the NAPL mixture molar volume, which is related to the inverse of the oil vapor density (Reid et al. 1987), given as

$$P_g^o = \frac{R^{o_i} T}{\upsilon - b} - \frac{\sum_{i,k=1}^{NC}\left(\chi^{o_i}\chi^{o_k}\sqrt{a^{o_i}a^{o_k}}\right)}{\upsilon^2 + 2b^{o_i}\upsilon - b^2} \tag{4.7}$$

where

$$a^{o_i} = \frac{0.45724\left(R^{o_i}\right)^2\left(T_c^{o_i}\right)^2}{P_c^{o_i}}\left(1+\left(0.37464+1.54226\omega-0.26992\omega^2\right)\left(1-\left(\frac{T}{T_c^{o_i}}\right)^{0.5}\right)\right)^2$$

$$b = \sum_{i=1}^{NC}\frac{0.7780 - R^{o_i}T_c^{o_i}}{P_c^{o_i}}$$

Gas-phase density equals the sum of the air, water and NAPL component densities:

$$\rho_g = \sum_{j=w,a,o}\rho_g^j \tag{4.8}$$

4.1.4 Gas-Phase Viscosity

Gas-phase viscosity depends on composition and temperature according to an extension of the Chapman-Enskog theory, which was proposed by Wilke for multicomponent gas mixtures at low densities [Bird et al. 1960]. This semi-empirical expression combines component vapor viscosities, gas-phase mole fractions, and component molecular weights into a gas mixture viscosity. Component vapor viscosities are computed separately as a function of temperature and pressure. Air component viscosity is determined as a function of temperature from empirical correlations [ASHRAE 1977], according to

$$\mu_g^a = 2.6693\times10^{-6}\frac{\left(M^a T\right)^{1/2}}{13.0827\left(1.188-\frac{0.051T}{97.0}\right)} \tag{4.9}$$

Water vapor viscosity is computed from the steam table formulations [ASME 1967]

$$\mu_g^w = \left[0.407T - 30.772 - \rho_g^w\left(3.4696\times10^{-3} - 5.9\times10^{-6}T\right)\right]\times10^{-7}$$

Oil vapor viscosity is determined for each component as a function of temperature and pressure from the Corresponding States method [Reid et al. 1987]

$$\mu_g^o = \frac{F_P^o}{\xi^o}\left[\begin{array}{l}0.807\left(T_r^o\right)^{0.618} - 0.357\exp\left(-0.449T_r^o\right)+\\ 0.340\exp\left(-4.058T_r^o\right)+0.018\end{array}\right]x10^{-7} \tag{4.10}$$

Values of F_P^o and ξ^o are defined in White and Oostrom (2000).

The computed component vapor viscosities are subsequently combined, according to the modified Chapman-Enskog theory to determine the gas-phase viscosity:

$$\mu_g = \sum_{j=w,a,o} \frac{\chi_g^j \mu_g^j}{\sum_{k=w,a,o} \chi_g^k \Phi_g^{jk}} \tag{4.11}$$

where,

$$\Phi_g^{jk} = \frac{1}{\sqrt{8}} \left(1 + \frac{M^j}{M^k} \right)^{-1/2} \left[1 + \left(\frac{\mu_g^j}{\mu_g^k} \right)^{1/2} \left(\frac{M^j}{M^k} \right)^{1/4} \right]^2 \tag{4.12}$$

4.1.5 Aqueous-Phase Viscosity

Aqueous phase viscosity is computed using the low solubility assumption as a function of temperature from an empirical expression for liquid water viscosity [Yaws et al. 1976], given as

$$\mu_L = \exp\left[-24.71 + \frac{4209.0}{T} + 0.04527T - 3.376E-05T^2 \right] x10^{-3} \tag{4.13}$$

4.1.6 NAPL-Phase Viscosity

Few estimation techniques exist for determining NAPL-phase viscosity for a mixture of oils. Moreover, many of the techniques require interaction parameters that account for the structure of the constituent molecules. Empirical relationships have been developed, and are usually based on an exponential dependence since linear expressions of mixture viscosities are generally not applicable. The STOMP simulator uses the Kendall and Monroe (1917) method to determine NAPL-phase viscosity for a mixture of liquid oils, which is expressed as an exponential dependence of the viscosity of each component, weighted by its mole fraction

$$\mu_n^{1/3} = \sum_{i=1}^{NC} \chi_n^i \mu_n^i \tag{4.14}$$

4.1.7 NAPL-Phase Component Fractions

The solubilities of air and water in the NAPL phase are assumed to be very small and are neglected in the STOMP simulator. Compositional NAPL contains mixtures of liquid-oil components. For compositional NAPL, the component partial pressures are the primary unknowns for all but one oil mass

conservation equation. Conversion between component partial pressure and component mole fraction in the NAPL phase is computed assuming equilibrium conditions using Raoult's law given as

$$P_g^o = \chi_n^o P_{sat}^o \tag{4.15}$$

4.2 Test Cases

A series of six test case simulations were conducted for both the STOMP water-oil and the STOMP water-oil-air mode to verify the proper implementation of multicomponent NAPL flow and transport. Each test case consists of a comparison with the equivalent single-component STOMP simulation and a limited sensitivity analysis where the effect of important fluid parameters such as viscosity and density are evaluated. A description of the six cases is presented in Table 4.1.

Table 4.1. Description of Test Cases for Multicomponent NAPL Formulation

Case No.	Objective	Description
1	demonstrate NAPL redistribution in a closed west-east horizontal system	1-m-long horizontal column; unsaturated system; initial NAPL gradient = -1000 Pa/m; three-component NAPL with same fluid properties Initial NAPL mole fractions of components: Case 1a: 1, 0, 0 Case 1b: 0, 1, 0 Case 1c: 0, 0, 1 Case 1d – 1h: 0.3, 0.2, 0.5 Viscosity of NAPL components is 1 cP except: Case 1e: Viscosity component 1 is 5 cP Case 1f: Viscosity component 2 is 5 cP Case 1g: Viscosity component 3 is 5 cP Density of NAPL components is 1.2 g/cm^3 except: Case 1h: Density of all components is 1.5 g/cm^3
2	demonstrate NAPL redistribution in a closed south-north horizontal system	1-m-long horizontal column; unsaturated system; initial NAPL gradient = -1000 Pa/m; three-component NAPL with same fluid properties Initial NAPL mole fractions of components: Case 2a: 1, 0, 0 Case 2b: 0, 1, 0 Case 2c: 0, 0, 1 Case 2d – 2h: 0.3, 0.2, 0.5 Viscosity of NAPL components is 1 cP except: Case 2e: Viscosity component 1 is 5 cP Case 2f: Viscosity component 2 is 5 cP Case 2g: Viscosity component 3 is 5 cP Density of NAPL components is 1.2 g/cm^3 except: Case 2h: Density of all components is 1.5 g/cm^3

Table 4.1. (contd)

Case No.	Objective	Description
3	test of introducing NAPL through Neumann and Dirichlet boundary conditions and through source injection in horizontal column	Horizontal 1-m-long column. Unsaturated. Three-component NAPL with same fluid properties. Viscosity 1 cP. Density 1.2 g/cm^3. Fluid injection period is 4 hours at the west site of the domain. Mole fractions 0.5, 0.5, 0. Case 3a: Injection of 100 mL using Neumann boundary condition Case 3b: Injection of 138.3 mL using Dirichlet boundary condition Case 3c: Injection of 100 mL using source
4	test of introducing NAPL through Neumann and Dirichlet boundary conditions into vertical column	Vertical 1-m-long column. Unsaturated with water table 10 cm from bottom. Three-component NAPL with same fluid properties. Viscosity 1 cP. Density 1.2 g/cm^3. Mole fractions 0.5, 0.5, 0. Fluid injection period is 4 hours. Case 4a: Injection of 100 mL using Neumann boundary condition at top Case 4b: Injection of 100 mL using Neumann boundary condition at bottom Case 4c: Injection of 180 mL using Dirichlet boundary condition at top Case 4d: As Case 4a with mole fraction 0.33, 0.33, 0.34 Case 4e: As Case 4a with viscosity of first two components 5 cP Case 4f: As Case 4a with viscosity of first component 5 cP Case 4g: As Case 4a with density of first two components 1.5 g/cm^3. Case 4h: As Case 4a with density of first component 1.5 g/cm^3. Case 4i: As Case 4a with permeability increased by factor 10. Case 4j: As Case 4i with permeability decreased by factor 10.
5	injection and redistribution of NAPL in heterogeneous system; testing of mass and mole fraction distributions	Horizontal 1-m-long saturated column. 10-cm long coarse sand zone in center. 45-cm low-permeability zones at either end. Three-component NAPL with same fluid properties. Viscosity 1 cP. Density 1.2 g/cm^3. Mole fractions 0.5, 0.5, 0 for 3 components. Fluid injection period is 4 hours into low-permeability zone, followed by 1 week redistribution without flushing. After that, the NAPL is dissolved by west-east moving groundwater. Case 5a: Injection of 100 mL. Case 5b: As Case 5a with molecular weight of component 2 decreased by factor 2 Case 5c: As Case 5a with injection of NAPL with mass fractions of 0.5, 0.5, 0.0 for 3 components.
6	injection and redistribution of NAPL in two-dimensional unsaturated system	1 x 1 m domain. Unsaturated with water table 10 cm from bottom. Three-component NAPL with same fluid properties. Viscosity 1 cP. Density 1.2 g/cm^3. Mole fractions 0.5, 0.5, 0. Fluid injection period is 4 hours. Case 6a: Injection of 100 mL light NAPL (0.8 g/cm^3) from 10-cm long source zone on top. Stagnant groundwater Case 6b: As Case 6a with moving groundwater (gradient 0.005). Case 6c: As Case 6a with injection of DNAPL (1.2 g/cm^3)

4.2.1 Cases 1 and 2

Cases 1 and 2 involve redistribution of NAPL in closed horizontal systems. For the single-component version of the STOMP simulator, input on the NAPL properties is provided in the Volatile Organic Properties Card, as shown below for Case 1a. The last three lines in this card provide information on fluid density, viscosity, and Henry's constant. Details on all the variables in this card can be found in White et al. (2006).

```
------------------------------------------------------------------------------------------
~Volatile Organic Properties Card
# Card ID: nc_mo_sc_case1a
NAPL,
260.7602,g/mol,164.2,K,268.7,K,425.0,K,
43.3,bar,221.0,cm^3/mol,0.270,0.195,0.0,debyes,
-1.687e+0,3.419e-1,-2.340e-4,6.335e-8,
Equation 5,0.20892e+2,0.30247e+04,-0.64044e+02,
Constant,1.2,g/cm^3,
Constant,1.0,cP,
1.0e9,Pa,
------------------------------------------------------------------------------------------
```

Information on the fluid properties for the NAPL components in the multicomponent version are provided in the NAPL Component Properties Card. In the example below, for Case 1a, the average properties of the composite NAPL are the same as for the NAPL used in the single-component card above since the assigned properties of NAPL1, NAPL2, and NAPL3 are identical as for the NAPL in the single-component card.

```
------------------------------------------------------------------------------------------
~NAPL Component Properties Card
# Card ID: nc_mo_mc_case1a
3,
NAPL1,
260.7602,g/mol,164.2,K,268.7,K,425.0,K,
43.3,bar,221.0,cm^3/mol,0.270,0.195,0.0,debyes,
-1.687e+0,3.419e-1,-2.340e-4,6.335e-8,
Equation 5,0.20892e+2,0.30247e+04,-0.64044e+02,
Constant,1.2,g/cm^3,
Constant,1.0,cP,
1.0e9,Pa,
NAPL2,
260.7602,g/mol,164.2,K,268.7,K,425.0,K,
43.3,bar,221.0,cm^3/mol,0.270,0.195,0.0,debyes,
-1.687e+0,3.419e-1,-2.340e-4,6.335e-8,
Equation 5,0.20892e+2,0.30247e+04,-0.64044e+02,
Constant,1.2,g/cm^3,
Constant,1.0,cP,
1.0e9,Pa,
NAPL3,
```

```
260.7602,g/mol,164.2,K,268.7,K,425.0,K,
43.3,bar,221.0,cm^3/mol,0.270,0.195,0.0,debyes,
-1.687e+0,3.419e-1,-2.340e-4,6.335e-8,
Equation 5,0.20892e+2,0.30247e+04,-0.64044e+02,
Constant,1.2,g/cm^3,
Constant,1.0,cP,
1.0e9,Pa,
---------------------------------------------------------------------------------------
```

The initial variation in NAPL saturation, as shown in Figure 4.1 for both the single-component and multicomponent version of Case 1, is the result of the NAPL pressure gradient imposed on the system in the Initial Conditions Card. This card is shown below for the multicomponent simulation. The NAPL pressure at the westernmost node is 101050 Pa, with a gradient of -1000 Pa/m over the domain. Since the NAPL pressure is less than atmospheric, the system is unsaturated (i.e., the gas saturation is greater than zero). As expected, the NAPL saturation over time becomes constant over the horizontal column. At all shown times, the results of the single component and multicomponent simulations are identical. Based on the properties of the NAPLs used in these simulations, both simulations should produce the same results.

```
---------------------------------------------------------------------------------------
~Initial Conditions Card
# Card ID: ic_mo_mc_case1a
5,
Aqueous Pressure,98825,Pa,,,,,,,1,20,1,1,1,1,
NAPL Pressure,101050,Pa,-1000,1/m,,,,,1,20,1,1,1,1,
Oil NAPL Mass Fraction,NAPL1,1.0,,,,,,,,1,20,1,1,1,1,
Oil NAPL Mass Fraction,NAPL2,0.0,,,,,,,,1,20,1,1,1,1,
Oil NAPL Mass Fraction,NAPL3,0.0,,,,,,,,1,20,1,1,1,1,
---------------------------------------------------------------------------------------
```

Figure 4.2 shows NAPL saturations at t = 30 days for Case 1a, 1e, 1f, and 1g. Case 1a has the NAPL with the highest viscosity and therefore moves the slowest towards equilibrium. For Cases 1e, 1f, and 1g, one of the three components has a viscosity of 5 cP, while the other two components have a viscosity of 1 cP. Case 1f has the lowest high-viscosity NAPL mole fraction and therefore the NAPL is redistributing the fastest, followed by Case 1e and Case 1g. The results shown in Figure 4.2 indicate that the viscosity computations for mixtures have been implemented correctly.

The results from Case 2 (not shown), are always identical to the results for Case 1. The matching results indicate that NAPL redistribution in both horizontal directions (west-east and south-north) was implemented correctly.

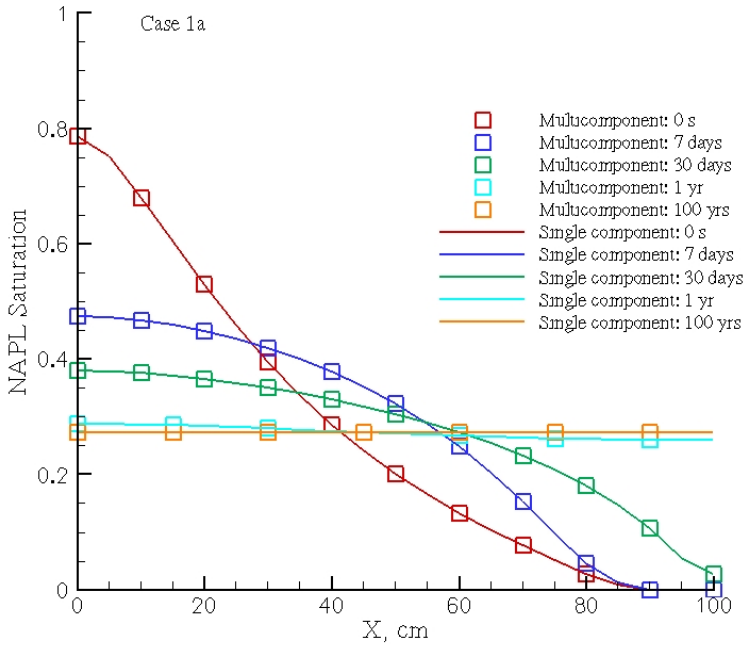

Figure 4.1. Comparison of NAPL Saturations Computed with the Single Component and Multicomponent versions of STOMP for Case 1a

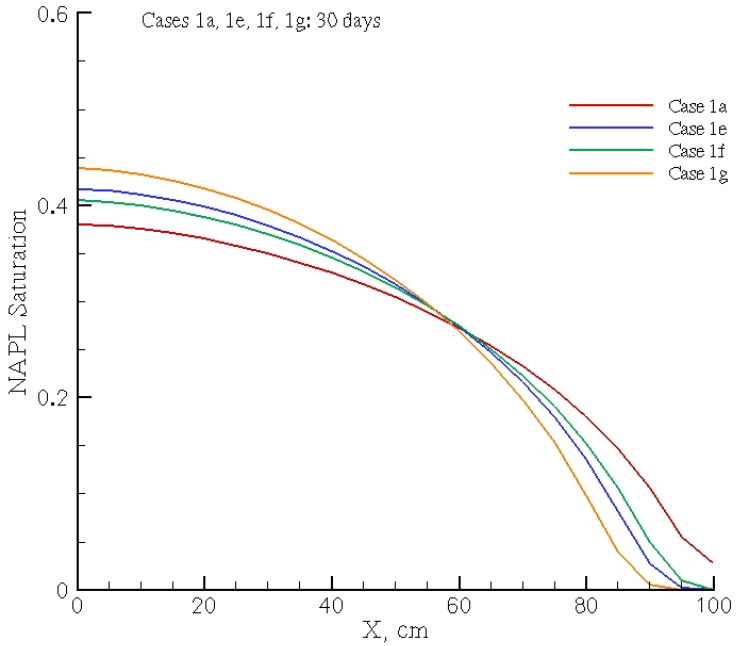

Figure 4.2. NAPL Saturations at t = 30 days for Cases 1a, 1e, 1f, and 1g

4.2.2 Case 3

Case 3 is a test of the proper implementation of NAPL Neumann (constant flux; Case 3a), Dirichlet (constant head; Case 3b) boundary conditions, and NAPL injection through a source (Case 3c). The imposed boundary conditions and NAPL source injection are listed in the three cards below for Case 3a, 3b, and 3c, respectively. For Cases 3a and 3c, 100 mL or NAPL are injected into the domain. For Case 3b, a total of 138 mL of NAPL makes it into the unsaturated porous medium. The results for Cases 3a, 3b, and 3c and comparisons with the equivalent single-component simulations are shown in Figures 4.4, 4.5, and 4.6, respectively. For all three cases, there is a perfect match between the single component and multicomponent simulations. As expected, the results for Cases 3a and 3c are identical, and for Case 3b, the NAPL saturations are higher that for the other two cases. The results demonstrate a correct implementation of the main NAPL boundary conditions and NAPL source injection.

```
---------------------------------------------------------------------------------------
~Boundary Conditions Card
# Card ID: bc_mo_mc_case3a
1,
West,Zero Flux,Aqueous Mass Fraction,Neumann,NAPL mass fraction,
1,1,1,1,1,1,2,
0,s,,Pa,,,,1.0,cm/hr,0.5,0.5,0.0,
4,hr,,Pa,,,,1.0,cm/hr,0.5,0.5,0.0,
---------------------------------------------------------------------------------------
```

```
---------------------------------------------------------------------------------------
~Boundary Conditions Card
# Card ID: bc_mo_mc_case3b
1,
West,Zero Flux,Aqueous Mass Fraction,Dirichlet NAPL,NAPL mass fraction,
1,1,1,1,1,1,2,
0,s,,Pa,,,,101325,Pa,0.5,0.5,0.0,
4,hr,,Pa,,,,101325,Pa,0.5,0.5,0.0,
---------------------------------------------------------------------------------------

---------------------------------------------------------------------------------------
~Source Card
# Card ID: sc_mo_mc_case3c
1,
NAPL Volumetric,1,1,1,1,1,1,2,Mass Fraction,
0,s,0.416666,ml/min,0.5,0.5,0.0,
4,hr,0.416666,ml/min,0.5,0.5,0.0,
---------------------------------------------------------------------------------------
```

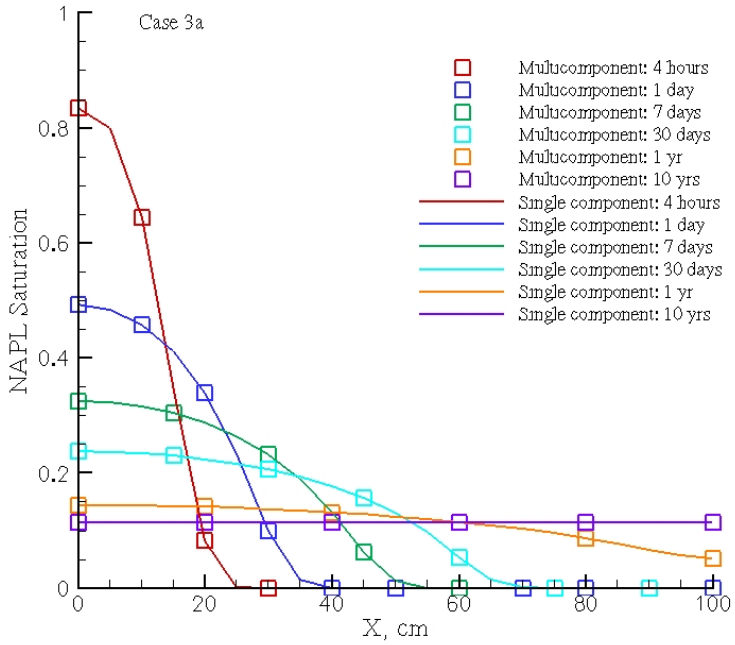

Figure 4.3. NAPL Saturations at Various Times for Multicomponent and Single Component Simulations (Case 3a)

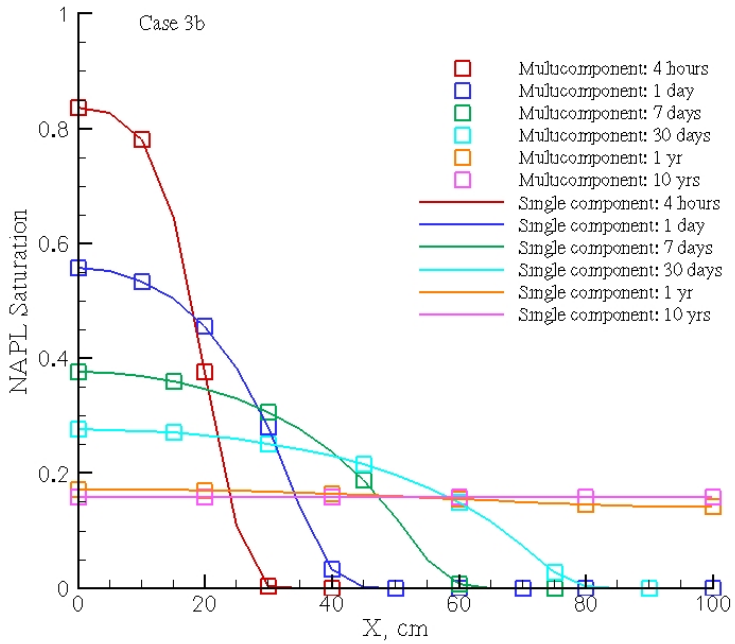

Figure 4.4. NAPL Saturations at Various Times for Multicomponent and Single Component Simulations (Case 3b)

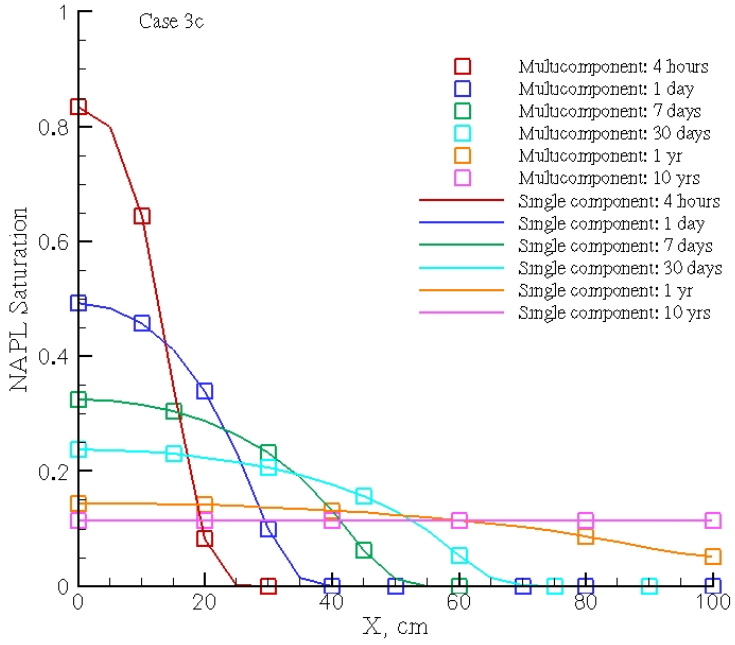

Figure 4.5. NAPL Saturations at Various Times for Multicomponent and Single Component Simulations (Case 3c)

4.2.3 Case 4

In Case 4, NAPL boundary conditions are tested in vertical systems. In Case 4a, 100 mL NAPL is injected from the top using a Neumann (constant flux) boundary condition. In Case 4b, 100 mL NAPL is injected through the bottom boundary using the same boundary condition. In Case 4c, a Dirichlet (constant head) boundary condition is used to inject ~180 mL NAPL into the unsaturated porous medium from the top. Comparisons with the equivalent single component simulations are shown in Figures 4.6, 4.7, and 4.8 for Cases 4a, 4b, and 4c, respectively. In all three cases, there is agreement with the single-component cases. In addition, the physical behavior of the three systems is consistent with expectations. In Cases 4a and 4c, the dense NAPL migrates downwards into the unsaturated zone and moves down all the way to the bottom of the column.

In Case 4d, the molar fractions of the three components are different from Case 4a. However, since the properties of the individual components are the same, the results should be identical, as is shown in Figure 4.9. In Cases 4e and 4f the viscosity of the NAPL was increased, resulting in a slower downward movement (Figure 4.1). As expected, the NAPL movement in Case 4e is the slowest since two NAPL components have a viscosity of 5 cP. The movement of the NAPL in Case 4f is in between Case 4a and Case 4e. Figure 4.11 shows the effect of increased density on downward NAPL movement. For Case 4g, the downward movement of the NAPL is the fastest, followed by Case 4h, and Case 4e. The shown results are according to expectation because the overall NAPL density is the highest in Case 4g, followed by Case 4h, and finally Case 4a. Finally, Figure 4.12 shows the effect on porous medium hydraulic conductivity on NAPL movement for the multicomponent formulation. In Case 4i, with the highest hydraulic conductivity, the NAPL moved the fastest to the bottom of the column. The slowest movement was observed for Case 4j, where the hydraulic conductivity was a factor of 10 less than for Case 4a.

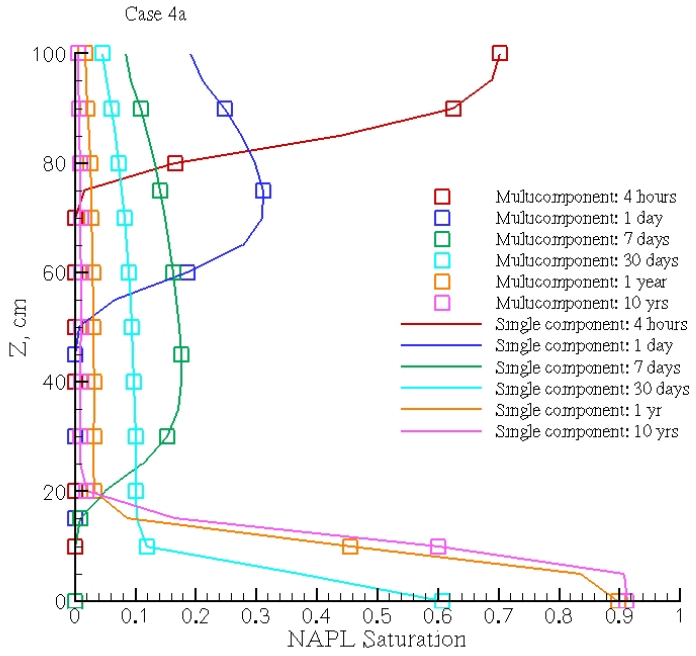

Figure 4.6. NAPL Saturations at Various Times for Multicomponent and Single Component Simulations (Case 4a)

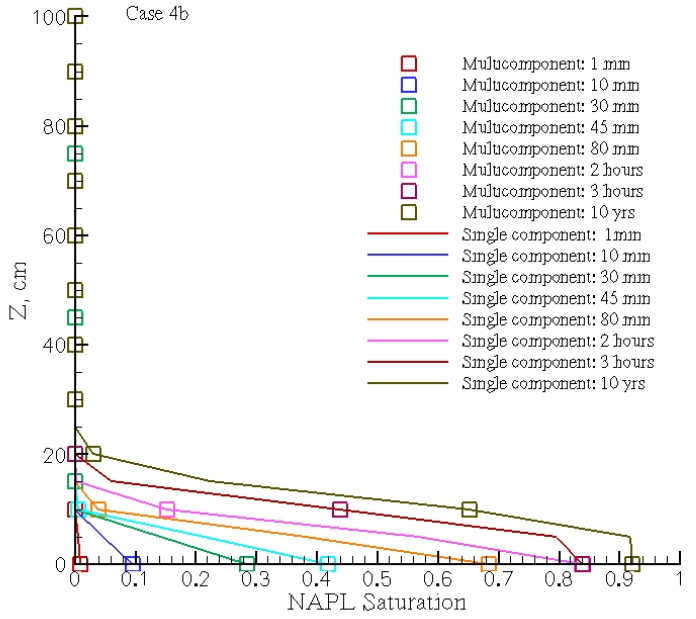

Figure 4.7. NAPL Saturations at Various Times for Multicomponent and Single Component Simulations (Case 4b)

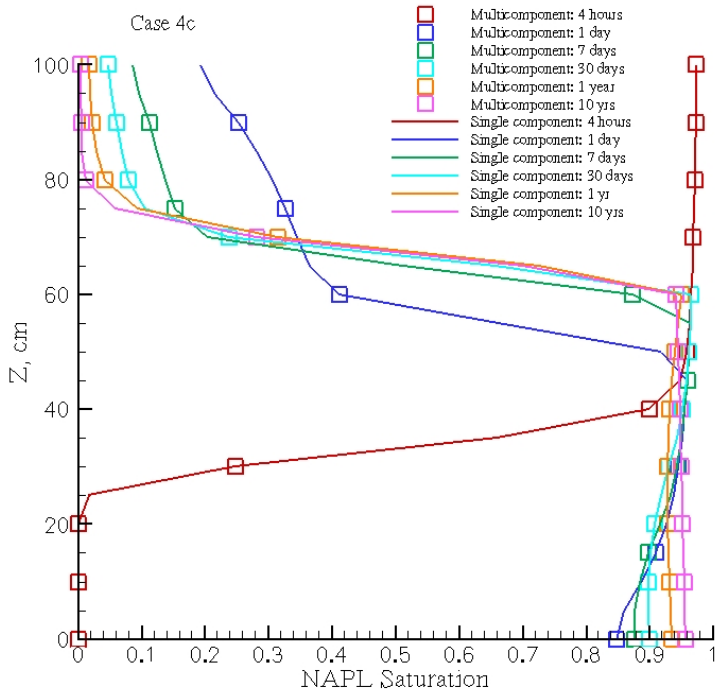

Figure 4.8. NAPL Saturations at Various Times for Multicomponent and Single Component Simulations (Case 4c)

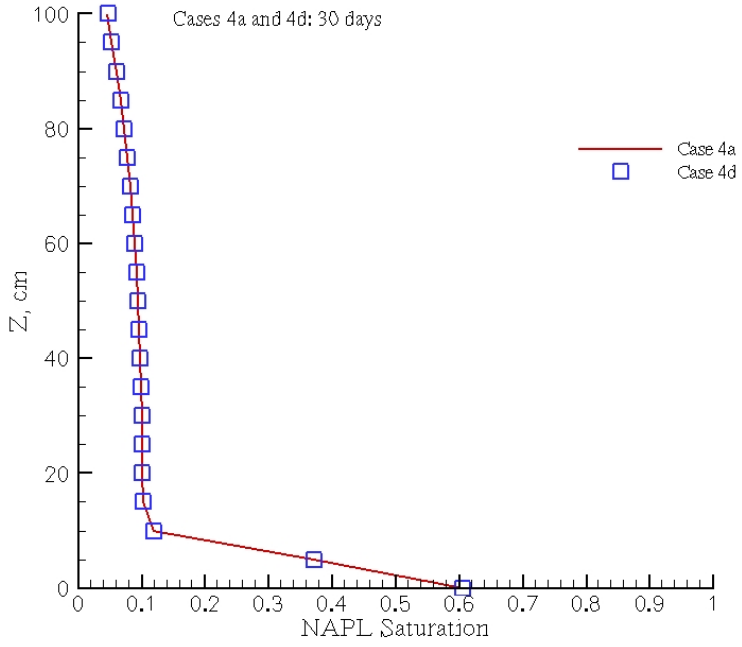

Figure 4.9. Comparison of Cases 4a and 4d at 30 Days

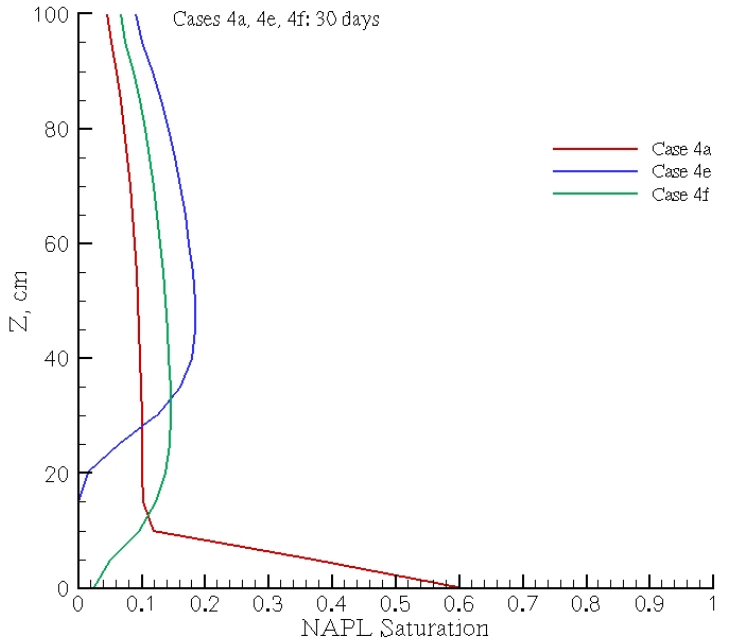

Figure 4.10. Comparison of Cases 4a, 4e, and 4f at 30 Days

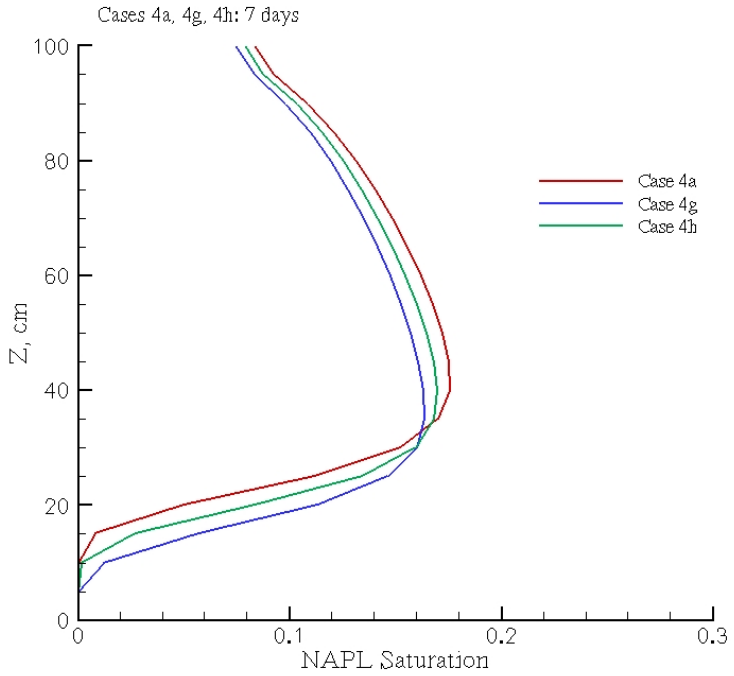

Figure 4.11. Comparison of Cases 4a, 4g, and 4h at 7 Days

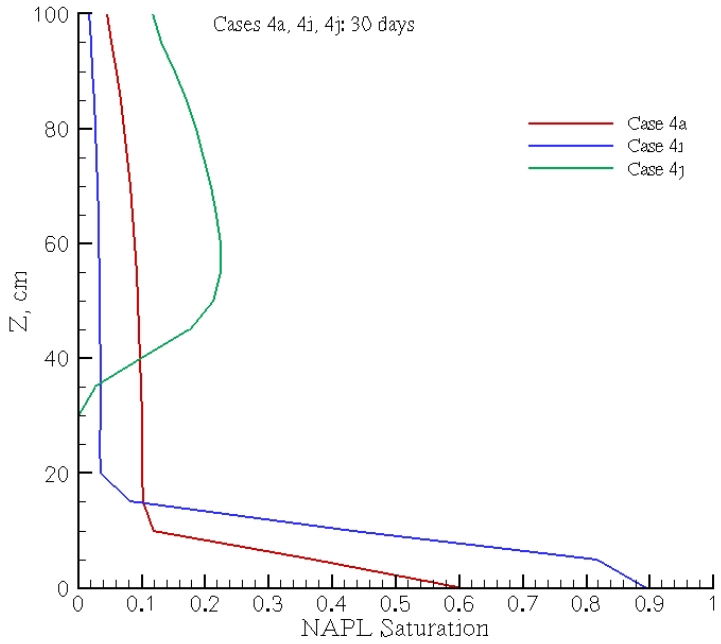

Figure 4.12. Comparison of Cases 4a, 4i, and 4j at 30 Days

4.2.4 Case 5

For Case 5, the effect of variable mass and mole fractions on flow and transport of a two-component NAPL is tested. For Case 5a, 100 mL NAPL was injected in a 10-cm long coarse sand. Adjacent on each side of the low permeability zone are two 45-cm zones with lower-permeability porous media. A comparison of results for the single component and multicomponent cases at various times are shown in Figures 4.13 and 4.14. The results of both simulations are the same, showing that multicomponent NAPL movement in a heterogeneous system has been incorporated correctly in the simulator.

For Case 5b the molecular weight of component DNAPL2 was set to be half of the molecular weight used in Case 5a, while keeping the mass fraction the same. As expected, the removal of the NAPL is slower than for Case 5a (Figure 4.15). The computed mass and mole fractions, shown at 4 weeks in Figure 4.16, are consistent with the lower molecular weight for component DNAPL2. The mass fractions, where NAPL is present in the system, for both component are at 0.5, while the mole fraction of DNAPL2 is 0.666 and that of DNAPL1 0.333.

In Case 5c, NAPL was injected with the same mole fraction (0.5) for each of the two components, while keeping all other conditions the same as for Case 5b. For this case, the mass removal is faster than for Case 5b but slower than for Case 5a.. The computed mole and mass fractions, shown in Figure 4.18, show equal mole fractions (0.5) at locations where NAPL is present. However, the computed mass fraction for DNAPL1 is 0.6666 and 0.333 for DNAPL2. These values are consistent with the imposed conditions on this simulation, again demonstrating correct implementation of NAPL distributions over mass or mole fractions.

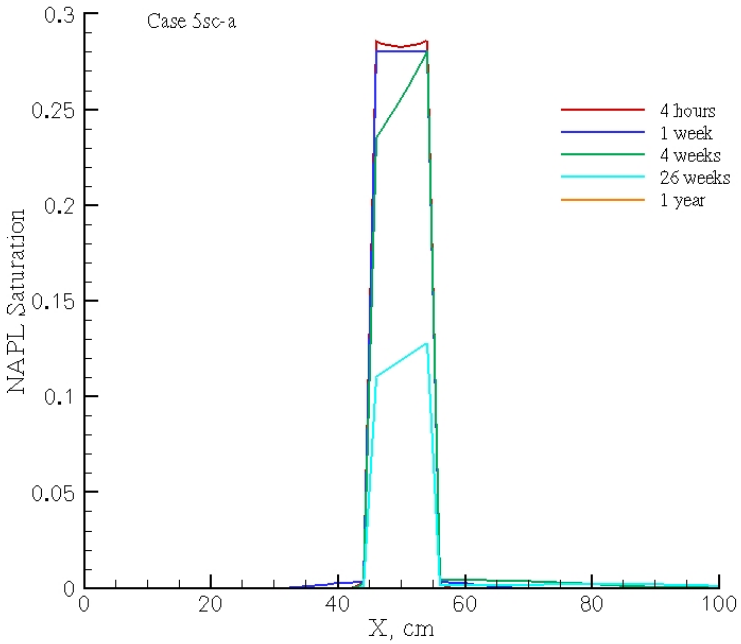

Figure 4.13. NAPL Saturations at Various Times for Case 5a Single Component Simulation

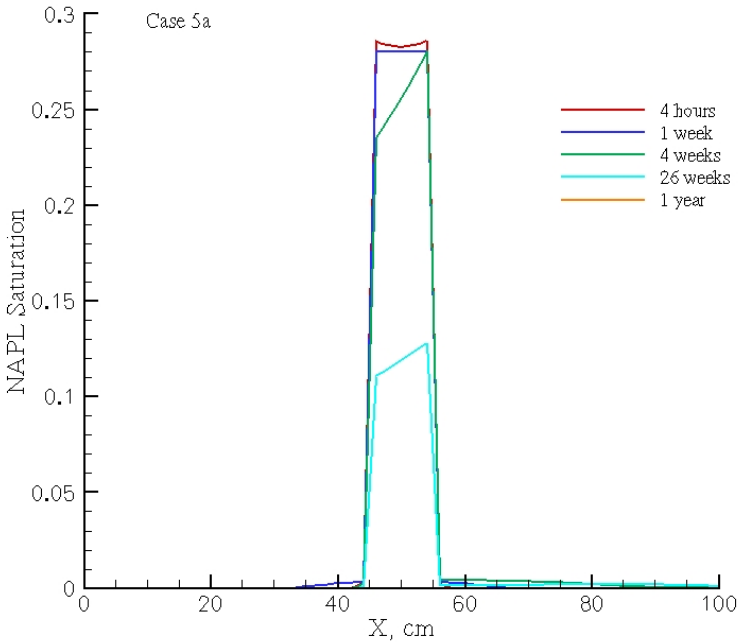

Figure 4.14. NAPL Saturations at Various Times for Case 5a Multicomponent Simulation

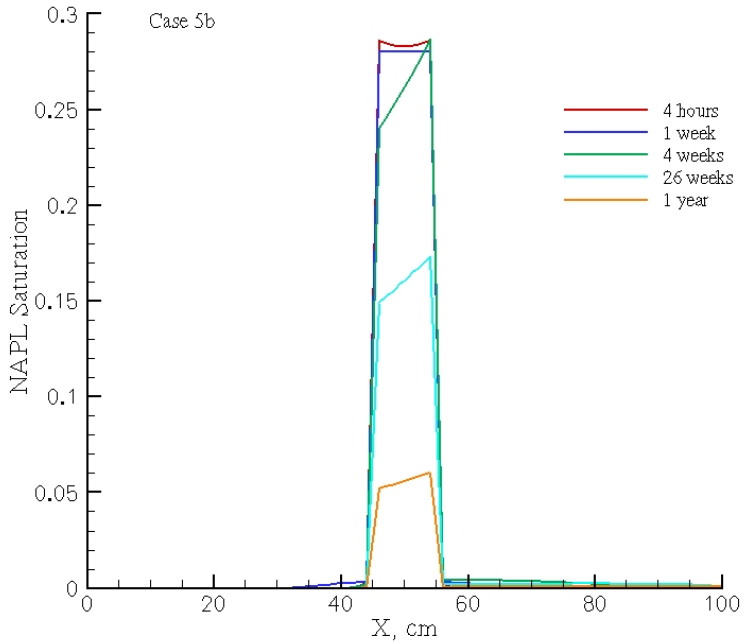

Figure 4.15. NAPL Saturations at Various Times for Case 5b Multicomponent Simulation

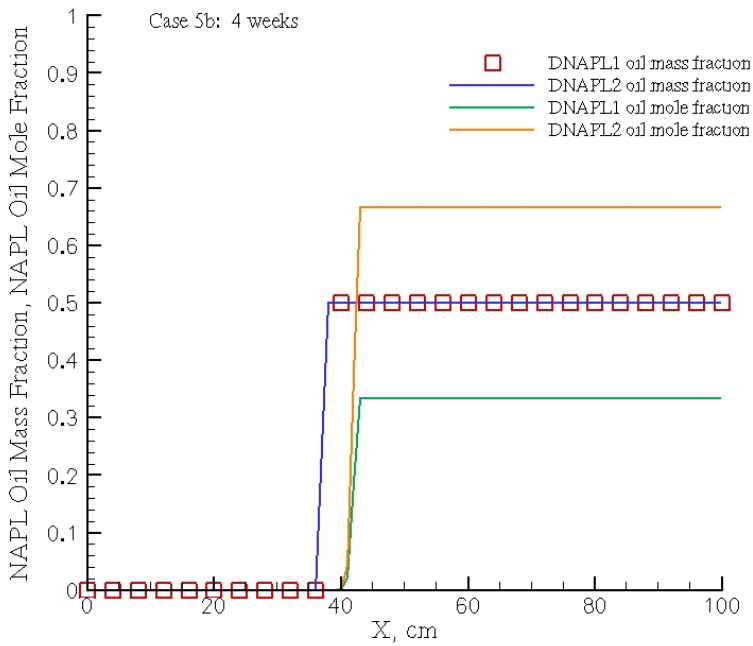

Figure 4.16. Mass and Mole Fractions for Case 5b at 4 Weeks

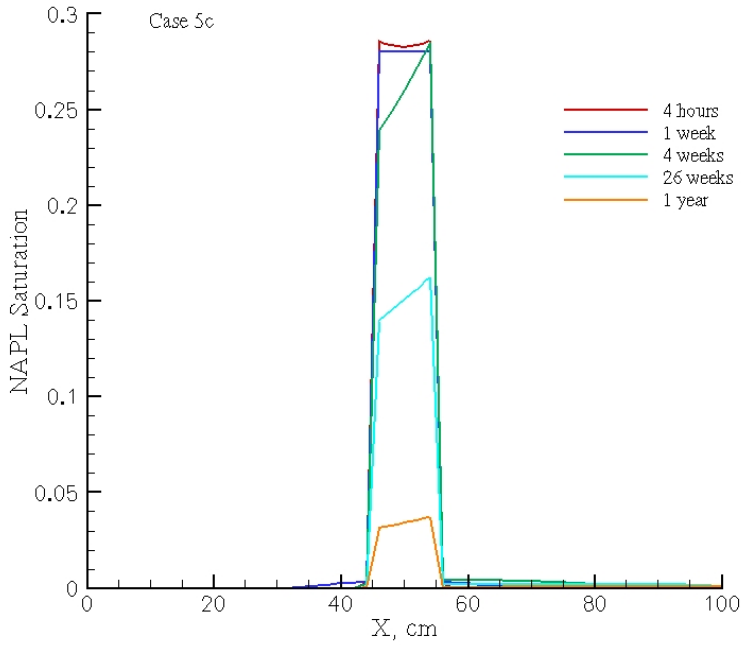

Figure 4.17. NAPL Saturations at Various Times for Case 5c Multicomponent Simulation

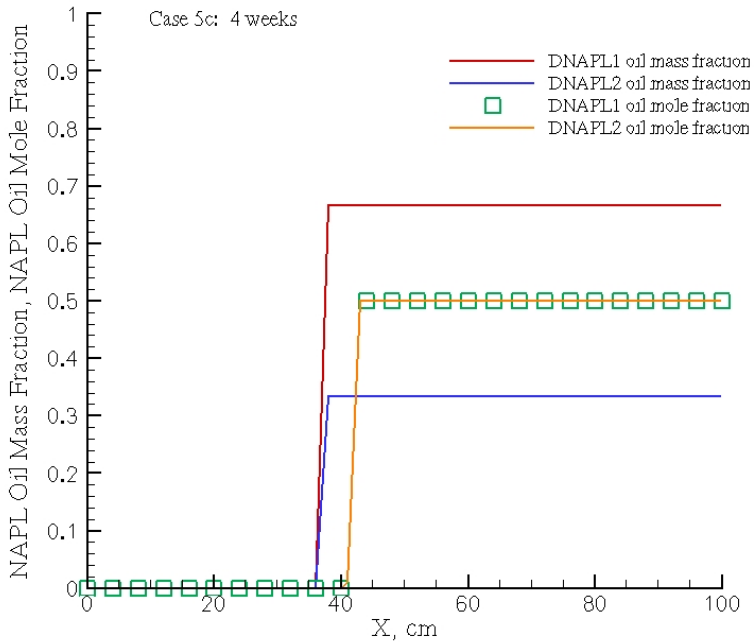

Figure 4.18. Mass and Mole Fractions for Case 5c at 4 Weeks

4.2.5 Case 6

The simulations in Case 6 involve infiltration and redistribution of NAPL in a variably saturated two-dimensional system with a water table 10 cm from the bottom. The objective of the simulations for this case is to obtain the same results for the multicomponent and equivalent single-component scenarios. For Case 6a, a LNAPL with a density of 0.8 g/cm^3 is injected from a source zone at the top. The results at various times for both simulations are the same, as is illustrated by Figures 4.19 and 4.20. For Case 6b, moving groundwater from left to right was added to test dissolution of NAPL in a two-dimensional system. Again, the results for the single-component and multicomponent simulations (Figures 4.21 and 4.22) at all times are the same, indicating correct implementation of the dissolution algorithms. Finally, in Case 6c, a DNAPL with a density of 1.2 g/cm^3 is injected under the same conditions as for Case 5a. The results show (Figures 4.23 and 4.24) that the DNAPL infiltrated faster than the LNAPL in Case 6a. The comparison between single-component and multicomponent NAPL behavior is again favorable, showing that multidimensional NAPL flow and transport has incorporated correctly into the STOMP simulator.

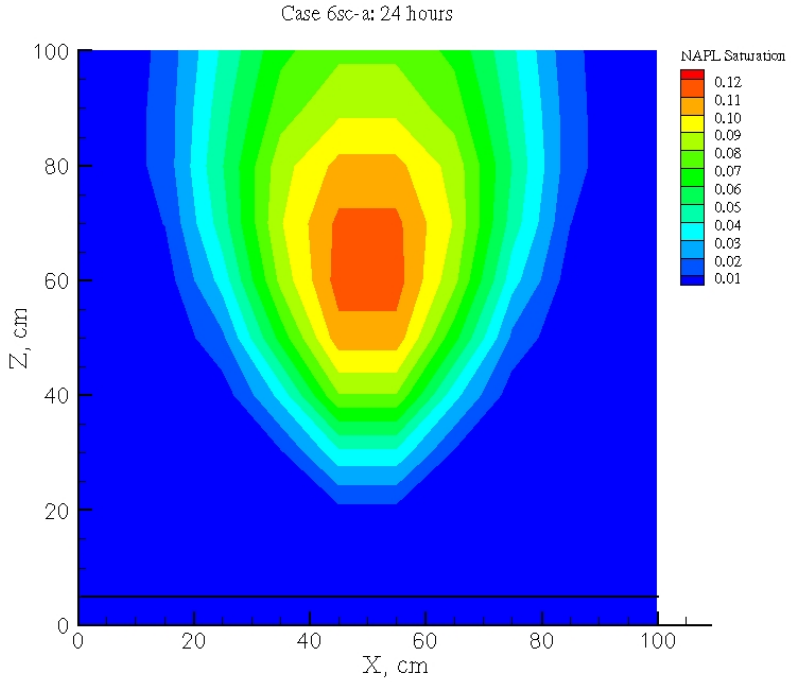

Figure 4.19. NAPL Saturations at 24 Hours for Case 6a Single Component Simulation

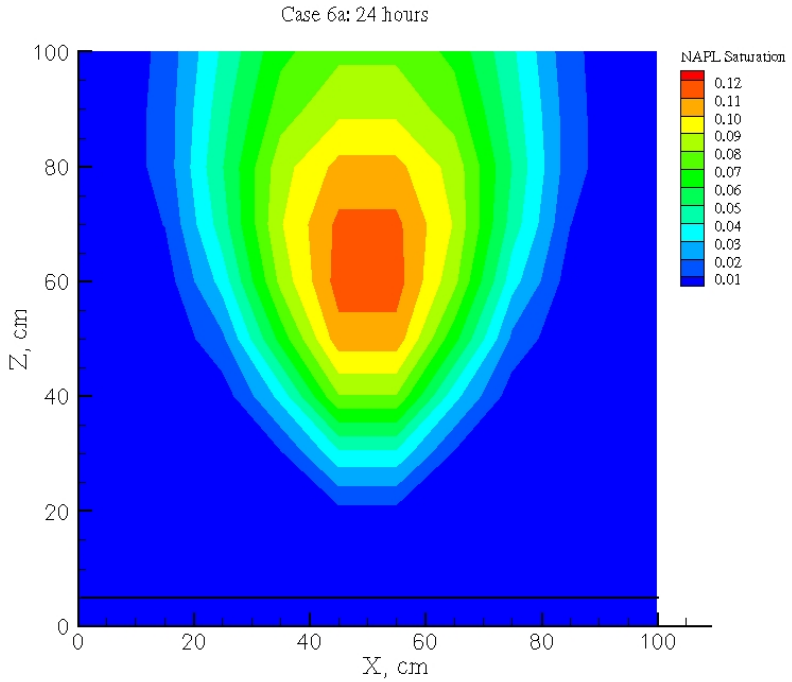

Figure 4.20. NAPL Saturations at 24 Hours for Case 6a Multicomponent Simulation

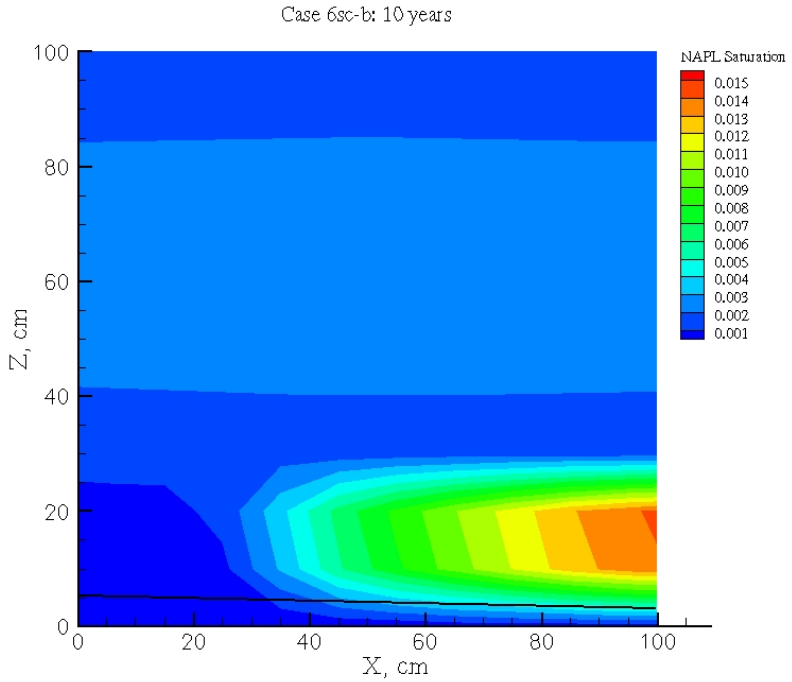

Figure 4.21. NAPL Saturations at 10 Years for Case 6b Single Component Simulation

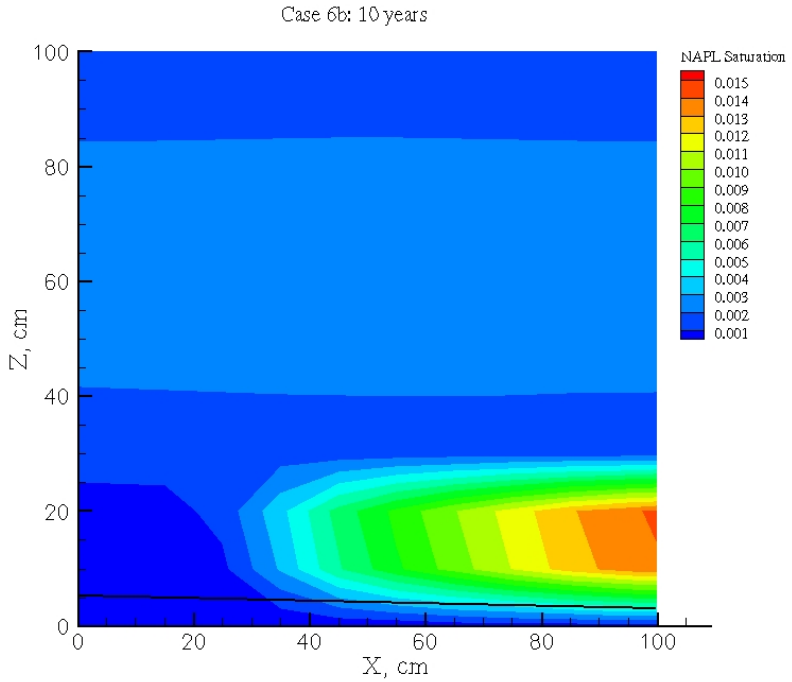

Figure 4.22. NAPL Saturations at 10 Years for Case 6b Multicomponent Simulation

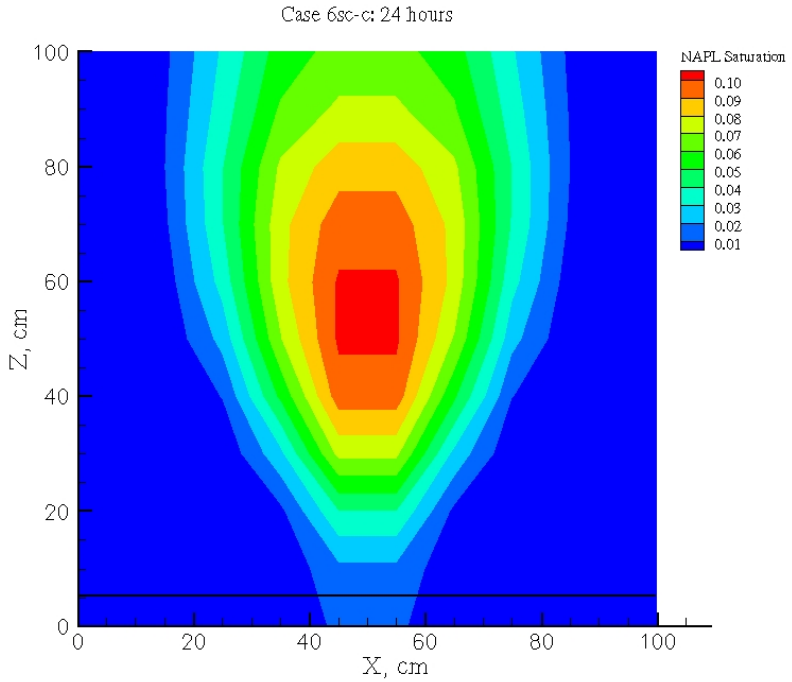

Figure 4.23. NAPL Saturations at 24 Hours for Case 6c Single Component Simulation

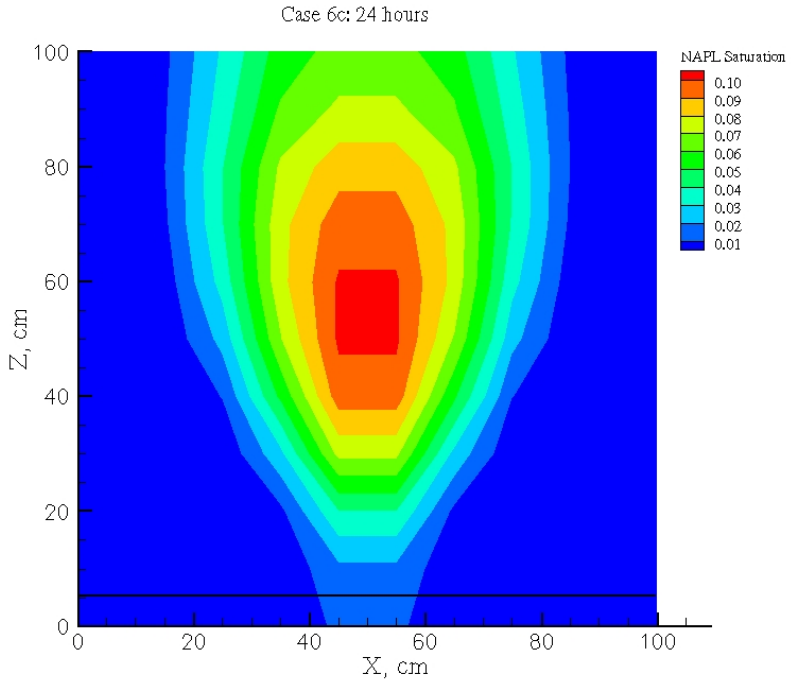

Figure 4.24. NAPL Saturations at 24 Hours for Case 6c Multicomponent Simulation

4.2.6 Test Summary

The above test results show that the multicomponent models behave correctly and adequately describe the physical processes of NAPL multicomponent flow and transport.

5.0 Summary and Conclusions

Previous numerical simulation results with the STOMP simulator have overestimated the effect of soil vapor extraction (SVE) on subsurface CT, showing rapid removal of considerably more CT than has actually been recovered so far. These previous multiphase simulations modeled CT mass transfer between phases based on equilibrium partitioning. Equilibrium volatilization can overestimate volatilization because mass transfer limitations present in the field are not considered. Previous simulations were also conducted by modeling the NAPL as a single component, CT. In reality, however, the NAPL mixture disposed of at the Hanford site contained several non-volatile and nearly insoluble organic components, resulting in time-variant fluid properties as the CT component volatilized or dissolved over time. Simulation of CT removal from a DNAPL mixture using single-component DNAPL properties typically leads to an overestimation of CT removal.

In this report, numerical implementation of kinetic volatilization and multicomponent DNAPL flow and transport into the STOMP simulator (White and Oostrom, 2006) is described. The kinetic volatilization models incorporated into the code were selected from recent literature and include the Wilkins et al. (1995), the van der Ham and Brouwers (1998), and the Yoon et al. (2002) models. The multicomponent flow and transport model incorporated into the code is based on fluid property averaging formulae obtained from the literature. The results of several test cases are presented and explained. The addition of these two major code enhancements increases the ability of the STOMP simulator to model complex subsurface flow and transport processes involving CT at the Hanford site.

6.0 References

Abriola LM, KD Pennell, WJ Weber, Jr., JR Lang, and MD Wilkins. 1999. *Persistence and interphase mass transfer of organic contaminants in the unsaturated zone: Experimental observations and mathematical modeling.* p. 210–234. *In* J.Y. Parlange and J.W. Hopmans (ed.) Vadose Zone Hydrology: Cutting across disciplines. Oxford University Press, New York.

Abriola LM, SA Bradford, J Lang, and CL Gaither. 2004. "Volatilization of Binary Nonaqueous Phase Liquid Mixtures in Unsaturated Porous Media." *Vadose Zone Journal*. 3:645–655.

Anwar AHMF, TH Tien, Y Inoue, and F Takagi. 2003. "Mass Transfer Correlation for Nonaqueous Phase Liquid Volatilization in Porous Media." *Environ. Sci. Technol.* 37:1277-1283.

Armstrong JE, EO Frind, and RD McClellan. 1994. "Nonequilibrium mass transfer between the vapor, aqueous, and solid phases in unsaturated soils during vapor extraction." *Water Resour. Res.* 30(2):355-368.

ASHRAE. 1977. *ASHRAE handbook and product directory, 1977 fundamentals.* American

Society of Heating, Refrigerating, and Air-Conditioning Engineers, Inc., New York.

ASME. 1967. *Thermodynamic and transport properties of steam.* The American Society of

Mechanical Engineers, United Engineering Center, New York.

Baehr A 1987. "Selective transport of hydrocarbons in the unsaturated zone due to aqueous and vapor phase partitioning." *Water Resour. Res.* 23(10):1926-1938.

Baehr AL, GE Hoag, and MC Marley. 1989. "Removing volatile contaminants from the unsaturated zone by inducing advective air-phase transport." *J. Contam. Hydrol.* 4:1-26.

Bohy M, L Dridi, G Schafer, and O Razakarisoa. 2006. "Transport of a mixture of chlorinated solvent vapors in the vadose zone of a sandy aquifer: Experimental study and numerical modeling." *Vadose Zone J.* 5:539-553.

Brooks RH and AT Corey. 1964. "Hydraulic Properties of Porous Media." *Hydrol. Pap. 3*, Civil Engineering Department, Colorado State University, Fort Collins, Colorado.

Brusseau ML, Z Zhang, NT Nelson, G Tick, and M Oostrom. 2002. "Dissolution of a nonuniformly distributed immiscible liquid: Condition dependent mass transfer coefficients." *Environ. Sci. Technol.* 36:1033–1041.

Burdine NT. 1953. "Relative Permeability Calculations from Pore-Size Distribution Data." *Petr. Trans., Am. Inst. Mining Metall. Eng*. 198:71-77.

Clement TP, TR Gautam, KK Lee, MJ Truex, GB Davis. 2004. "Modeling of DNAPL-Dissolution, Rate-Limited Sorption and Biodegradation Reactions in Groundwater Systems." *Bioremediation Journal.* 8(1-2):47-64.

Corapcioglu MY, and AL Baehr. 1987. "A compositional multiphase model for groundwater contamination by petroleum products 1. Theoretical conditions." *Water Resour. Res.* 23(1):191-200.

Falta RW 2000. “Numerical modeling of kinetic interphase mass transfer during air sparging using a dual-media approach.” *Water Resour. Res.* 36(12):3391-3400.

Harper, B. M., W. H. Stiver, and R. G. Zytner. 2003. “Nonequilibrium Nonaqueous Phase Liquid Mass Transfer Model for Soil Vapor Extraction Systems.” *Journal of Environmental Engineering.* 129(8):745-754.

Imhoff P, P Jaffé, and G Pinder. 1994. “An experimental study of complete dissolution of a nonaqueous phase liquid in saturated porous media.” *Water Resour. Res.* 30(2):307-320.

Imhoff P, P Jaffé, and G Pinder. 1994b. Correction to "An experimental study of complete dissolution of a nonaqueous phase liquid in saturated porous media." *Water Resour. Res.* 30(10): 2871-2871.

Johnson PC, MW Kemblowski, and JD Colthart. 1990. “Quantitative analysis for the cleanup of hydrocarbon-contaminated soils by in-situ soil venting.” *Ground Water.* 28(3):413-429.

Kendall J and KP Monroe. 1917. J. Am. Chem. Soc. 39:1787 – 1806.

Lee S-H, I-T Yeom, K-H Ahn, and J Khim. 2001. “Nonequilibrium mass transfer of multi-component NAPL in a soil column venting.” *Environmental Technology.* 22:741-748.

Leverett MC. 1941. “Capillary Behavior in Porous Solids.” *Trans. Soc. Pet. Eng. AIME* 142:152-169.

Lingineni S and VK Dhir. 1992. “Modeling of soil venting processes to remediate unsaturated soils.” *Journal of Environmental Engineering*. 118(1):135-152.

Mackay DM, MB Bloes, and KM Rathfelder. 1990. *Laboratory studies of vapor extraction for remediation of contaminated soil.* Paper presented at Conference on Subsurface Contamination by Immiscible Liquids, Int. Assoc. of Hydrogeol., Calgary, Alberta, Canada.

Miller CT, MM Poirier-McNeill, and AS Mayer. 1990. “Dissolution of trapped nonaqueous phase liquids: Mass transfer characteristics.” *Water Resour. Res.* 26(11):2783-2796.

Mualem Y. 1976. “A New Model for Predicting the Hydraulic Conductivity of Unsaturated Porous Media.” *Water Resour. Res*. 12:513-522.

Nambi IM, and SE Powers. 2003. “Mass transfer correlations for nonaqueous phase liquid dissolution from regions with high initial saturations.” *Water Resour. Res.* 39(2):1030. doi:10.1029/2001WR000667.

Oostrom M, C Hofstee, and JH Dane. 1997. “Light Nonaqueous-Phase Liquid Movement in a Variably Saturated Sand.” *Soil Science Society of America J*. 61:1547-1554.

Oostrom M and RJ Lenhard. 1998. “Comparison of relative permeability-saturation-pressure parametric models for infiltration and redistribution of a light nonaqueous phase liquid in sandy porous media.” *Adv. in Water Resour*. 21:145-157.

Oostrom M, C Hofstee, RC Walker, and JH Dane. 1999. “Movement and Remediation of Trichloro-ethylene in a Saturated, Heterogeneous Porous Medium. 1. Spill Behavior and Initial Dissolution.” *J. of Contaminant Hydrol*. 37:159-178.

Oostrom M, ML Rockhold, PD Thorne, GV Last, and MJ Truex. 2006a. *Carbon Tetrachloride Flow and Transport in the Subsurface of the 216-Z-9 Trench at the Hanford Site: Heterogeneous Model Development and Soil Vapor Extraction Modeling.* PNNL-15914, Pacific Northwest National Laboratory, Richland, Washington.

Oostrom M., ML Rockhold, PD Thorne, GV Last, and MJ Truex. 2006b. *Carbon Tetrachloride Flow and Transport in the Subsurface of the 216-Z-18 Crib and 216-Z-1A Tile Field at the Hanford Site: Multifluid Flow Simulations and Conceptual Model Update.* PNNL-16198, Pacific Northwest National Laboratory, Richland, Washington.

Oostrom M, ML Rockhold, PD Thorne, GV Last, MJ Truex, and VJ Rohay. 2007a. "Carbon tetrachloride flow and transport in the subsurface of the 216-Z-9 trench at the Hanford Site: Multifluid flow modeling and conceptual model update." *Vadose Zone J.* 971-984.

Oostrom M, PD Thorne, F Zhang, GV Last, and MJ Truex. 2007b. *Modeling of carbon tetrachloride flow and transport in the subsurface of the 200 West disposal sites: Large-scale model configuration and local-scale prediction of future carbon tetrachloride distribution beneath the 216-Z-9 disposal site.* PNNL-17181, Pacific Northwest National Laboratory, Richland, Washington.

Parker JC, AK Katyal, JJ Kaluarachchi, RJ Lenhard, TJ Johnson, K Jayaraman, K Unlu, and JL Zhu. 1991. *Modeling multiphase organic chemical transport in soils and ground water.* Rep. EPA/600/2-91/042, U.S. Environ. Protect. Agency, Washington, D.C.

Peng DY and DB Robinson. 1976. "A New Two-Constant Equation of State." *Ind. Eng. Chem.Fundam.* 15:59-64.

Powers SE, LM Abriola, and WJ Weber Jr. 1992. "An experimental investigation of NAPL dissolution in saturated subsurface systems: Steady-state mass transfer rates" *Water Resour. Res.* 28(10):2691 – 2706.

Powers SE, LM Abriola, and WJ Weber Jr. 1994. "An experimental investigation of NAPL dissolution in saturated subsurface systems: Transient mass transfer rates." *Water Resour. Res.* 30(2):321–332.

Rahbeh ME and RH Mohtar. 2006. "Modeling multiphase contaminant transport in porous media using first-order mass transfer kinetics." *American Society of Agricultural and Biological Engineers.* 49(6):1935-1945.

Rahbeh ME and RH Mohtar. 2007. "Application of multiphase transport models to field remediation by air sparging and soil vapor extraction." *Journal of Hazardous Materials.* 143:156-170.

Rainwater K, MR Zaman, BJ Claborn, and HW Parker. 1989. *Experimental and modeling studies of in situ volatilization: Vapour-liquid equilibrium or diffusion-controlled process?* Paper presented at Conference on Petroleum Hydrocarbons and Organic Chemicals in Ground Water: Prevention, Detection and Restoration, Natl. Well Water Assoc./Am. Pet. Inst., Houston, Tex.

Rathfelder KM. 1989. "Numerical simulation of soil vapor extraction systems." Ph.D. thesis provided to the University of California at Los Angeles.

Rathfelder K, WW-G Yeh, and D Machay. 1991. "Mathematical simulation of soil vapor extraction systems: model development and numerical examples." *J. Contam. Hydrol.* 8:263-297.

Rathfelder KM, JR Lang, LM Abriola. 2000. “A numerical model□MISER/for the simulation of coupled physical, chemical and biological processes in soil vapor extraction and bioventing systems.” *Journal of Contaminant Hydrology.* 43:239–270.

Reid RC, JM Prausnitz, and BE Poling. 1987. *The properties of gases and liquids.*

Fourth edition, McGraw-Hill Book Company, New York.

Saba T and TH Illangasekare. 2000. “Effect of groundwater flow dimensionality on mass transfer from entrapped nonaqueous phase liquid contaminants.” *Water Resour. Res.* 36:971–979.

van der Ham AGJ and HJH Brouwers. 1998. “Modelling and experimental investigation of transient, nonequilibrium mass transfer during steam stripping of a nonaqueous phase liquid in unsaturated porous media.” *Water Resour. Res.* 34 (1):47–54.

van Wylen GJ and RE Sonntag. 1978. *Fundamentals of classical thermodynamics.*

2nd edition, revised printing, John Wiley & Sons, Inc., New York.

Wakao N and S Kaguei. 1982. *Heat and mass transfer in packed beds.* Gordon and Breach Science, New York, 1982.

White MD and M Oostrom. 2000. *STOMP Subsurface Transport Over Multiple Phases Version 2.0 Theory Guide.* Pacific Northwest National Laboratory, Richland, Washington.

White MD and M Oostrom. 2000. *STOMP Subsurface Transport Over Multiple Phases*

Version 2.0 Theory Guide. PNNL-12030 UC-2010, Pacific Northwest National

Laboratory, Richland, Washington.

White MD, M Oostrom, ML Rockhold, and M Rosing. 2008. “Scalable modeling of carbon tetrachloride migration in the deep vadose zone at the Hanford Site using the STOMP simulator.” *Vadose Zone J.* 7:654-666.

Wilkins MD, LM Abriola, and KD Pennell. 1995. “An experimental investigation of rate-limited nonaqueous phase liquid volatilization in unsaturated porous media: steady state mass transfer.” *Water Resour. Res.* 31(9):2159–2172.

Wilson, DE, RE Montgomeery, and MR Sheller. 1987. “A mathematical model for removing volatile subsurface hydrocarbons by miscible displacement.” *Water Air Soil Pollut.* 33:231-255.

Wilson DJ, AN Clarke, and JH Clarke. 1988. “Soil clean up by in-situ aeration, 1. Mathematical modeling.” *Sep. Sci. Technol.* 23(10-11):991-1037.

Yaws CL, JW Miller, PN Shah, GR Schorr, and PM Patel. 1976. *Chem. Eng. Sci.*

Yoon H, JH Kim, HM Liljestrand, and J Khim. 2002. “Effect of water content on transient nonequilibrium NAPL–gas mass transfer during soil vapor extraction.” *Journal of Contaminant Hydrology.* 54:1-18.

Appendix A

STOMP Input File for the Base Case Kinetic Volatilization Simulation Scenario Using the Wilkins Model

Appendix A

STOMP input file for the base case kinetic volatilization simulation scenario using the Wilkins model.

```
#-------------------------------------------------------------
~Simulation Title Card
# Card ID: tc_b
#-------------------------------------------------------------
1,
STOMP-WOA Kinetic Volatilization/Dissolution Test,
Fred Zhang, Mart Oostrom,
PNNL,
June 2008,
,
1,
Carbon tetrachloride Volatilization/Dissolution,
#-------------------------------------------------------------
~Solution Control Card
# Card ID: scc_ki
#-------------------------------------------------------------
Normal,
Water-Oil-Air w/ Kinetic Volatilization,
3,
0,  d,0.1,d,0.0001,d,0.001,d,1.25,8,1.e-6,
0.1,d,1,  d,0.01,  d,0.01, d,1.25,8,1.e-6,
1.0,d,10, d,0.1,   d,0.1,  d,1.25,8,1.e-6,
10000,
Variable,
Constant,0.9e-6,m^2/s,0.9e-6,m^2/s,
0,
#-------------------------------------------------------------
~Grid Card
# Card ID: gc_b
#-------------------------------------------------------------
Cartesian,
3,3,3,
0,m,3@0.1,m,
0,m,3@0.1,m,
0,m,3@0.1,m,
#-------------------------------------------------------------
~Rock/Soil Zonation Card
# Card ID: rsc_b
#-------------------------------------------------------------
2,
Sand1,1,3,1,3,2,3,
Sand2,1,3,1,3,1,1,
#-------------------------------------------------------------
~Mechanical Properties Card
# Card ID: mpc_b
```

```
#-------------------------------------------------------------
Sand1,2650,kg/m^3,0.4,0.4,,,Millington and Quirk,
Sand2,2650,kg/m^3,0.4,0.4,,,Millington and Quirk,
#-------------------------------------------------------------
~Hydraulic Properties Card
# Card ID: hpc_b
#-------------------------------------------------------------
Sand1,100.0,hc m/day,100.0,hc m/day,100.0,hc m/day,
Sand2,100.0,hc m/day,100.0,hc m/day,100.0,hc m/day,
#-------------------------------------------------------------
~Saturation Function Card
# Card ID: sfc_b
#-------------------------------------------------------------
72.0,dynes/cm,,,35.43,dynes/cm,
Sand1,Van Genuchten,2.5,1/m,2.0,0.10,72.0,dynes/cm,,
Sand2,Van Genuchten,2.5,1/m,2.0,0.10,72.0,dynes/cm,,
#-------------------------------------------------------------
~Aqueous Relative Permeability Card
# Card ID: arp_b
#-------------------------------------------------------------
Sand1,Mualem,,
Sand2,Mualem,,
#-------------------------------------------------------------
~NAPL Relative Permeability Card
# Card ID: nrp_b
#-------------------------------------------------------------
Sand1,Constant,0.0,
Sand2,Constant,0.0,
#-------------------------------------------------------------
~Gas Relative Permeability Card
# Card ID: grp_b
#-------------------------------------------------------------
Sand1,Mualem,,
Sand2,Mualem,,
#-------------------------------------------------------------
~Oil Properties Card
# Card ID: opc_b
#-------------------------------------------------------------
Carbontetrachloride,
153.82,g/mol,250.,K,349.9,K,556.4,K,
45.6,bar,275.9,cm^3/mol,0.272,0.193,0.0,debyes,
4.072e+1,2.0496e-1,-2.27e-4,8.843e-8,
Constant,12000,Pa,
Constant,1623,kg/m^3,
Constant,0.97e-3,Pa s,
1.3062e8,Pa,
#-------------------------------------------------------------
~Oil Transport Card
# Card ID: ot_wi
#-------------------------------------------------------------
Sand1,0.2,cm,0.02,cm,linear kd,0.0,m^3/kg,0.02,cm,
```

```
Sand2,0.2,cm,0.02,cm,linear kd,0.0,m^3/kg,0.02,cm,
Wilkins Model,
#-------------------------------------------------------------
~Initial Conditions Card
# Card ID: ic_b
#-------------------------------------------------------------
4,
Aqueous Pressure, 81725.0,Pa,,,,,-9793,1/m, 1,3,1,3,1,3,
Gas Pressure,    101350.0,Pa,-100.0,1/m,,,-11.71,1/m,1,3,1,3,1,3,
NAPL Pressure,    -1.e9,  Pa,,,,,,,         1,3,1,3,1,3,
NAPL Pressure,    96425.0,Pa,,,,,,,         2,2,2,2,2,2,
#-------------------------------------------------------------
~Boundary Conditions Card
# Card ID: bc_b
#-------------------------------------------------------------
2,
west,aq hydraulic gradient,gas hydraulic gradient,napl dirichlet,
1,1,1,3,1,3,1,
0,d, 81725.0,Pa,,,101355.0,Pa,,,-1.e9,Pa,
east,aq hydraulic gradient,gas hydraulic gradient,napl dirichlet,
3,3,1,3,1,3,1,
0,d, 81725.0,Pa,,,101325.0,Pa,,,-1.e9,Pa,
#-------------------------------------------------------------
~Source Card
# Card ID: src_b
#-------------------------------------------------------------
0,
#-------------------------------------------------------------
~Output Options Card
# Card ID: oc_b
#-------------------------------------------------------------
1,
2,2,2,
10,1,day,m,4,6,6,
14,
rock/soil type,,
phase condition,,
integrated gas oil mass,g,
integrated aqueous oil mass,g,
integrated oil mass,g,
aqueous saturation,,
napl saturation,,
napl pressure,pa,
gas pressure,pa,
oil aqueous concentration,g/L,
oil gas concentration,g/L,
oil gas mole fraction,,
xnc gas volumetric flux,m/min,
xnc aqueous volumetric flux,m/min,
5,
0.0,d,
```

1.0,d,
2.0,d,
5.0,d,
10.0,d,
11,
rock/soil type,,
phase condition,,
aqueous saturation,,
napl saturation,,
napl moisture content,,
napl pressure,,
gas pressure,pa,
oil aqueous concentration,g/L,
oil gas concentration,g/L,
oil gas mole fraction,,
no restart,,
#----------
~Surface Flux Card
Card ID: sfl_b
#----------
8,
Gas total-oil mass flux,g/d,g,west ,1,1,1,3,1,3,
Gas total-oil mass flux,g/d,g,east ,3,3,1,3,1,3,
Dissolved oil mass flux,g/d,g,west ,1,1,1,3,1,3,
Dissolved oil mass flux,g/d,g,east ,3,3,1,3,1,3,
Gas Volumetric flux,L/d,L,west ,1,1,1,3,1,3,
Gas Volumetric flux,L/d,L,east ,3,3,1,3,1,3,
Aqueous Volumetric flux,L/d,L,west ,1,1,1,3,1,3,
Aqueous Volumetric flux,L/d,L,east ,3,3,1,3,1,3,

Appendix B

STOMP Input File for Case 1a Multicomponent Simulation

Appendix B:

STOMP input file for Case 1a multicomponent simulation

```
~Simulation Title Card
# Card ID: st_mo_mc_case1a
1,
Multicomponent Problem 1-MC-a,
Mart Oostrom,
PNNL,
May 2008,
PM,
5,
Horizontal,
Redistribution of NAPL saturations,
Zero Flux Boundary Conditions,
All three NAPL components have identical properties,
Results from this problem should be identical to Problem 1-SC,

~Solution Control Card
# Card ID: sc_mo_mc_case1a
Normal,
Water-Oil,
1,
0,yr,100,yr,1,s,0.1,yr,1.25,12,1.e-6,
#1,
10000,
Variable Aqueous Diffusion,
,

~Grid Card
# Card ID: gc_mo_mc_case1a
Cartesian,
20,1,1,
0,cm,20@5,cm,
0,cm,5,cm,
0,cm,5,cm,

~Rock/Soil Zonation Card
# Card ID: rs_mo_mc_case1a
1,
sand,1,20,1,1,1,1,

~Mechanical Properties Card
# Card ID: mp_mo_mc_case1a
sand,2650,kg/m^3,0.35,0.35,,,Millington and Quirk,

~Hydraulic Properties Card
# Card ID: hp_mo_mc_case1a
sand,1.0,hc m/day,,,,,
```

~Saturation Function Card
Card ID: sf_mo_mc_case1a
72.0,dynes/cm,,,32.0,dynes/cm,
#sand,Brooks and Corey,10,cm,2.0,0.02,72.0,dynes/cm,
sand,Van Genuchten,0.1,1/cm,3.0,0.02,72.0,dynes/cm,,,

~Aqueous Relative Permeability Card
Card ID: arp_mo_mc_case1a
#sand,Burdine,,
sand,Mualem,,

~NAPL Relative Permeability Card
Card ID: nrp_mo_mc_case1a
#sand,Burdine,,
sand,Mualem,,

~NAPL Component Properties Card
Card ID: nc_mo_mc_case1a
3,
NAPL1,
260.7602,g/mol,164.2,K,268.7,K,425.0,K,
43.3,bar,221.0,cm^3/mol,0.270,0.195,0.0,debyes,
-1.687e+0,3.419e-1,-2.340e-4,6.335e-8,
Equation 5,0.20892e+2,0.30247e+04,-0.64044e+02,(1,1,2-trichloroethane)
Constant,1.2,g/cm^3,
Constant,1.0,cP,
1.0e9,Pa,
NAPL2,
260.7602,g/mol,164.2,K,268.7,K,425.0,K,
43.3,bar,221.0,cm^3/mol,0.270,0.195,0.0,debyes,
-1.687e+0,3.419e-1,-2.340e-4,6.335e-8,
Equation 5,0.20892e+2,0.30247e+04,-0.64044e+02,(1,1,2-trichloroethane)
Constant,1.2,g/cm^3,
Constant,1.0,cP,
1.0e9,Pa,
NAPL3,
260.7602,g/mol,164.2,K,268.7,K,425.0,K,
43.3,bar,221.0,cm^3/mol,0.270,0.195,0.0,debyes,
-1.687e+0,3.419e-1,-2.340e-4,6.335e-8,
Equation 5,0.20892e+2,0.30247e+04,-0.64044e+02,(1,1,2-trichloroethane)
Constant,1.2,g/cm^3,
Constant,1.0,cP,
1.0e9,Pa,

~Initial Conditions Card
Card ID: ic_mo_mc_case1a
5,
Aqueous Pressure,98825,Pa,,,,,,,1,20,1,1,1,1,
NAPL Pressure,101050,Pa,-1000,1/m,,,,,1,20,1,1,1,1,
Oil NAPL Mass Fraction,NAPL1,1.0,,,,,,,,1,20,1,1,1,1,

Oil NAPL Mass Fraction,NAPL2,0.0,,,,,,,,1,20,1,1,1,1,
Oil NAPL Mass Fraction,NAPL3,0.0,,,,,,,,1,20,1,1,1,1,

~Output Options Card
Card ID: oo_mo_mc_case1a
5,
1,1,1,
5,1,1,
10,1,1,
15,1,1,
20,1,1,
1,1,yr,cm,6,6,6,
10,
aqueous pressure,Pa,
aqueous saturation,,
napl pressure,Pa,
napl saturation,,
oil NAPL mass fraction,NAPL1,,
oil NAPL mass fraction,NAPL2,,
oil NAPL mass fraction,NAPL3,,
oil aqueous concentration,NAPL1,,
oil aqueous concentration,NAPL2,,
oil aqueous concentration,NAPL3,,
4,
0,s,
7,d,
30,d,
1,yr,
10,
aqueous pressure,Pa,
aqueous saturation,,
napl pressure,Pa,
napl saturation,,
oil NAPL mass fraction,NAPL1,,
oil NAPL mass fraction,NAPL2,,
oil NAPL mass fraction,NAPL3,,
oil aqueous concentration,NAPL1,,
oil aqueous concentration,NAPL2,,
oil aqueous concentration,NAPL3,,

Distribution

No. of Copies

OFFSITE

R.S. Dinicola
U.S. Geological Survey
Washington Water Science Center
1210 Pacific Ave., Suite 600
Tacoma, WA 98402

ONSITE

3 **DOE Richland Operations Office**

J. G. Morse	A6-38
A. C. Tortoso	A6-38
Public Reading Room	H2-53

7 **Fluor Hanford, Inc.**

B. H. Ford	E6-35
D.S. Miller	E6-35
S. W. Petersen	E6-35
V. J. Rohay	E6-35
C. Sutton	E6-35
L. C. Swanson	E6-35
M. Tonkin	E6-35

No. of Copies

U.S. Environmental Protection Agency

D. E. Faulk	T4-04

Washington State Department of Ecology

D. Goswami	H0-57

10 **Pacific Northwest National Laboratory**

V.L. Freedman	K9-33
M. D. Freshley	K9-33
C. T. Kincaid	K9-33
M. Oostrom	K9-33
G. Tartakovsky	K9-33
M. J. Truex	K6-96
M.D. White	K9-33
F. Zhang	K9-33
Hanford Technical Library	P8-55

Pacific Northwest
NATIONAL LABORATORY

U.S. DEPARTMENT OF
ENERGY

902 Battelle Boulevard
P.O. Box 999
Richland, WA 99352
1-888-375-PNNL (7665)
www.pnl.gov